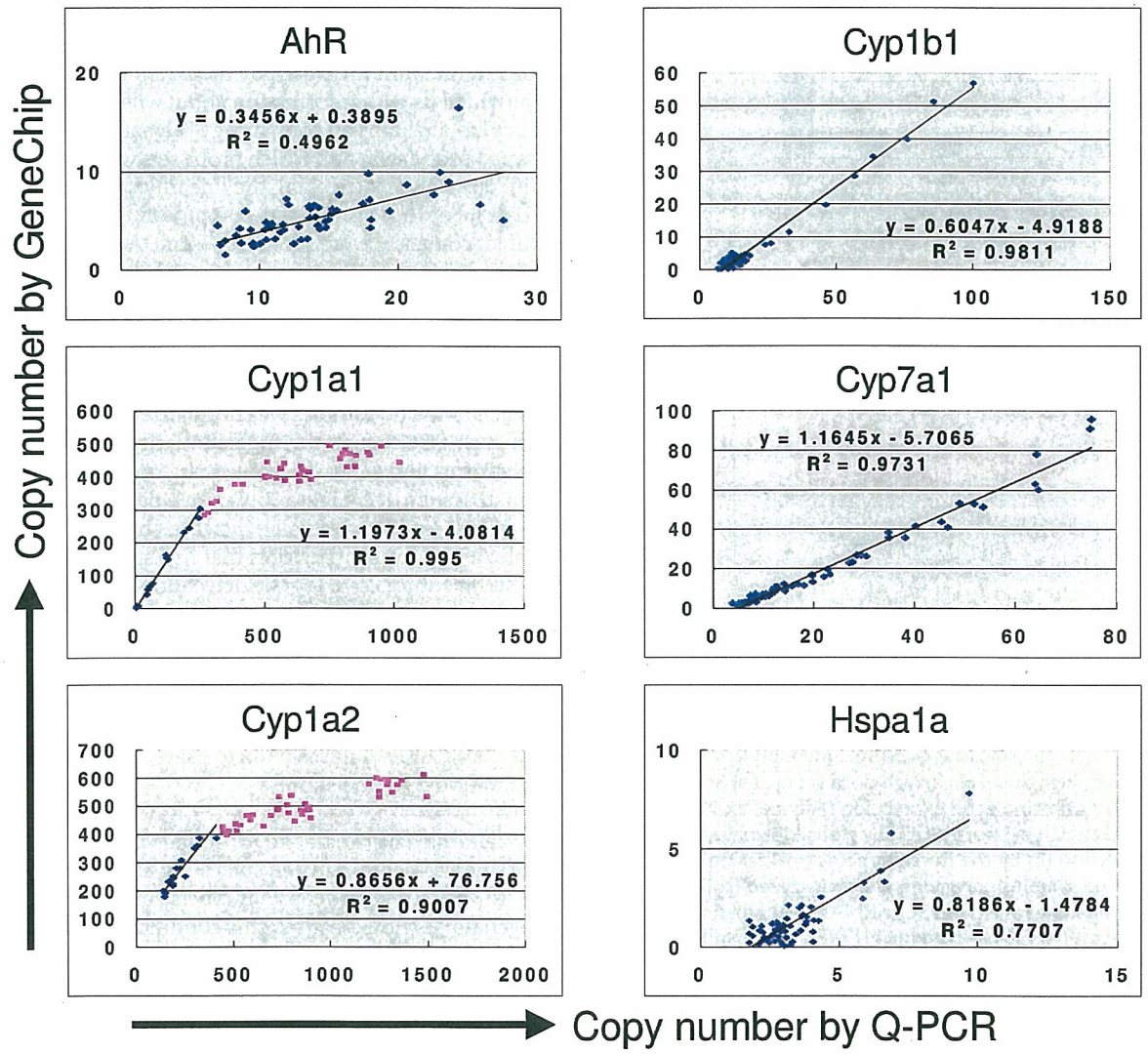

Figure 7
Conversion functions between Q-PCR and GeneChip. The data shown in Figure 5 as 3D surfaces are shown as a scatter plot (60 plots). The regression function can be used to convert Q-PCR to GeneChip and vice versa, with a level of certainty indicated by coefficient of correlation. It is noted that Cyp1a1 and Cyp1a2 became saturated above about 400 copies per cell in GeneChip system (indicated in pink plots). Cyp7a1 showed high linearity, indicating that the variation shown by the split +1sd and -1sd surfaces in Figure 5 reflected biological (animal) variation, not measurement errors.

Another important contribution of Percellome analysis is in the area of archived data in private and public domains. Firstly, Percellome data are the result of a simple linear transformation of the raw microarray data; preserving the distribution and order of the probe set data. Therefore, parametric or non-parametric methods should be able to align the data distribution and generate estimates of mRNA copy number of the non-spiked archival samples. Any archival samples that are re-measurable by Percellome method will greatly increase the accuracy of estimation. Secondly, percellome can provide appropriate bridging information between old and new versions of Affymetrix GeneChips, such as human HU-95 and HU-133, murine MU-74v2 and MOE430 series. This should also facilitate comparisons between newly generated and archived data.

The Percellome method was developed for a large-scale toxicogenomics project [13] using the Affymetrix GeneChip system. It was intended to compile a very large-scale database of comprehensive gene expression profiles in response to various chemicals from a series of experiments conducted over an extended time period. However, the method also proved to be useful for small-scale platforms such as 96 well plate-based Q-PCRs as shown above, and probably for small-scale targeted microarrays. In both cases, highly inducible or highly transcribed genes are likely to be selected. Therefore, the expression profiles may differ significantly among samples such that profile-dependent normalization (e.g. global normalization) may not be applicable. In such cases, the profile-independent nature of the Percellome method provides a robust normalization.

To demonstrate the profile-independence of the Percellome method, we chose an extreme case – the uterotrophic response assay (cf. Figure 6). The treated uteri were composed of hypertrophic cells with abundant cytoplasm whereas the untreated uteri were composed of hypoplastic cells with scant cytoplasm. This indicates that the uteri of untreated ovariectomized mice were quiescent, and that a majority of the inducible genes were probably transcriptionally inactive. Therefore, the identification of most genes as being induced by 2-fold or greater is reasonable and expected. In most *in vivo* experiments, the gene profiles of the samples are much more similar. However, there is always a set of genes that is found to be "increased" when analyzed on a "per one cell" basis that are declared to be "decreased" by global type normalization, or vice versa. Such increase/decrease calls made by the global type normalization can differ according to the normalization parameters. In both cases, the Percellome method can inform the researcher how much the expression profiles are distorted by the treatment, such as in the case of the uterotrophic assay. We also note that *in vitro* experiments such as cell-based studies tend to generate data similar to that of uterotrophic experiment.

Conclusion

Percellome data can be compared directly among samples and among different studies, and between different platforms, without further normalization. Therefore, "percellome" normalization can serve as a standard method for exchanging and comparing data across different platforms and among different laboratories. We hope that the Percellome method will contribute to transcriptome-based studies by facilitating data exchanges among laboratories.

Methods

Animal experiments

C57BL/6 Cr Slc (SLC, Hamamatsu, Japan) mice maintained in a barrier system with a 12 h photoperiod were used in this study. For the liver transcriptome experiments, twelve week-old male mice were given a single dose of the test compound by oral gavage, and the liver was sampled at 2, 4, 8 and 24 h post-gavage. For the uterotrophic experiment, 6 week old female mice were ovariectomized 14 days prior to the 7 day repeated subcutaneous injection of a test compound [12]. Animals were euthanized by exsanguination under ether anesthesia and the target organs were excised into ice-cooled plastic dishes. Tissue blocks weighing 30 to 60 mg were placed in an RNase-free 2 ml plastic tube (Eppendorf GmbH., Germany) and soaked in RNAlater (Ambion Inc., TX) within 3 min of the beginning of anesthesia. Three animals per treatment group were used and individually subjected to transcriptome measurement.

Sample homogenate preparation

The tissue blocks soaked in RNAlater were kept overnight at 4°C or until use. RNAlater was replaced in the 2 ml plastic tube with 1.0 ml of RLT buffer (Qiagen GmbH., Germany), and the tissue was homogenized by adding a 5 mm diameter Zirconium bead (Funakoshi, Japan) and shaking with a MixerMill 300 (Qiagen GmbH., Germany) at a speed of 20 Hz for 5 min (only the outermost row of the shaker box was used).

Direct DNA quantitation

Three separate 10 μl aliquots were taken from each sample homogenate to another tube and mixed thoroughly. A final 10 μl aliquot therefrom was treated with DNAse-free RNase A (Nippon Gene Inc., Japan) for 30 min at 37°C, followed by Proteinase K (Roche Diagnostics GmbH., Germany) for 3 h at 55°C in 1.5 ml capped tubes. The aliquot was transferred to a 96-well black plate. PicoGreen fluorescent dye (Molecular Probes Inc., USA) was added to each well, shaken for 10 seconds four times and then incubated for 2 min at 30°C. The DNA concentration was measured using a 96 well fluorescence plate reader with excitation at 485 nm and emission at 538 nm. λ phage DNA (PicoGreen Kit, Molecular Probes Inc., USA) was used as standard. Measurement by this PicoGreen method and the standard phenol extraction method correlated well (coefficient of correlation = 0.97, data not shown). The smallest sample size for reproducible and reliable DNA quantitation is about 5,000 cells that corresponds to a 6.75 dpc mouse embryo.

The grade-dosed spike cocktail (GSC)

The following five *Bacillus subtilis* RNA sequences were selected from the gene list of Affymetrix GeneChip arrays (AFFX-ThrX-3_at, AFFX-LysX-3_at, AFFX-PheX-3_at, AFFX-DapX-3_at, and AFFX-TrpnX-3_at) present in the MG-U74v2, RG-U34, HG-U95, HG-U133, RAE230 and MOE430 arrays: thrC, thrB genes corresponding to nucleotides 248–2229 of X04603; lys gene for diami-

nopimelate decarboxylase corresponding to nucleotides 350–1345 of X17013; pheB, pheA genes corresponding to nucleotides 2017–3334 of M24537, dapB, jojF, jojG genes corresponding to nucleotides 1358–3197 of L38424; TrpE protein, TrpD protein, TrpC protein corresponding to nucleotides 1883–4400 of K01391. The corresponding cDNAs were purchased from ATCC, incorporated into expression vectors, amplified in *E. coli* and transcribed using the MEGAscript kit (Ambion Inc., TX). The mRNA was purified using a MACS mRNA isolation kit (Miltenyi Biotec GmbH., Germany). The concentrations of spike RNAs in the GSC were in threefold steps, from 777.6 pM for AFFX-ThrX-3_at, 259.4 pM for AFFX-LysX-3_at, 86.4 pM for AFFX-PheX-3_at, 28.8 pM for AFFX-DapX-3_at, to 9.6 pM for AFFX-TrpnX-3_at. In general, the ratio depends on the linear range of the measurement system and the available number of spikes.

Setting of the "spike factor" and addition of GSC to a sample homogenate according to its DNA concentration

The GSC was added to the sample homogenates in proportion to their DNA concentrations, assuming that all cells contain a fixed amount of genomic DNA (g/cell) across samples. The amount of GSC added to each sample G (l) was given as

$$G = C * v * f \quad (l),$$

where C is the DNA concentration (g/l), v(l) is the volume of homogenate further used for RNA extraction and f (l/g) is the "spike factor", which is an adjustment factor to ensure that the sample is properly spiked by the GSC (cf. Figure 3). Spike factors have been pre-determined for various organs/tissues to reflect differences in their total RNA/genomic DNA ratios (cf. Table 1). In this way, five spike mRNA signals can properly cover the linear dose-response range of the platform. In practice, for the Affymetrix GeneChips, the spike factor is set so that the five GSC spikes cover the range of "Present" calls given by the Affymetrix system, which corresponds to approximately 80 to 7000 in raw readouts given by the Affymetrix MAS5.0 software. A raw readout of 10 by the current Affymetrix GeneChip system corresponds to approximately one copy per cell in mouse liver (spike factor = 0.2), whereas in mouse thymus (spike factor = 0.01) it corresponds to approximately 0.05 copy per cell. For Q-PCR, the same spike factor corresponds to Ct values ranging approximately from 17 to 27, which is well within the linear range of Q-PCR (data not shown).

"Per cell" normalization (Percellome normalization)

Since murine haploid genomic DNA is made of 2.5×10^9 base pairs and one base pair is approximately 600 Daltons (Da), the haploid genomic DNA weighs 1.5×10^{12} Da, corresponding to

$d = 5 \times 10^{-12}$ (g DNA per diploid cell).

Therefore, the cell number per liter of the sample homogenate (N) is given as

$$N = C/d \text{ (cells/l)}$$

where C is the DNA concentration (g/l).

On the other hand, the copy numbers of GSC RNAs in the homogenate are given as follows:

if Sj (mole/l) (j = 1,2,3,4,5) is the mole concentration of one of the five spike RNAs in the GSC solution and G(l) is the amount of GSC added to each homogenate, the mole concentrations of the spike RNAs in the homogenate (CSj) are given as,

$$CSj = Sj*C*f \text{ (mole/l)}.$$

The GSC RNAs in moles per cell (MSj) are given as

$$MSj = CSj/N$$

$$= Sj*C*f/(C/d)$$

$$= Sj*f*d \text{ (mole/cell)}$$

The copy numbers of the GSC RNAs per cell (NSj) are given as

$$NSj = MSj*A$$

$$= Sj*f*d*A \text{ (copies per diploid cell)}$$

where A is Avogadro's number.

As a result, the GSC spikes AFFX-TrpnX-3_at, AFFX-DapX-3_at, AFFX-PheX-3_at, AFFX-LysX-3_at and AFFX-ThrX-3_at correspond approximately to 5.8, 17.3, 52.0, 156.0 and 468.1 copies per cell (per diploid DNA template) for mouse liver sample homogenates, where the spike factor = 0.2. It is our observation that the RNA/DNA ratios are virtually constant across polyploid hepatocytes (data not shown).

For each Q-PCR plate or GeneChip, the coefficients, α, β, γ and δ of functions {1} or {2} are determined from the GSC values using the least-square method. The signal values or Ct values of all the other mRNAs measured are then converted to copy numbers per cell by {3} or {4}, i.e. the inverses of functions {1} or {2}.

Table 2: Primers for Q-PCR

Gene	Forward	Reverse
AFFX-TrpnX-3_at	TTCTCAGCGTAAAGCAATCCA	GCAAATCCTTTAGTGACCGAATACC
AFFX-DapX-3_at	TCAGCTAACGCTTCCAGACC	GGCCGACAGATTCTGATGACA
AFFX-PheX-3_at	GCCAATGATATGGCAGCTTCTAC	TGCGGCAGCATGACCATTA
AFFX-LysX-3_at	CCGCTTCATGCCACTGAATAC	CCGGTTCGATCCAAATTTCC
AFFX-ThrX-3_at	CCTGCATGAGGATGACGAGA	GGCATCGGCATATGGAAAC
Ahr_1450695_at	CAGAGACCACTGACGGATGAA	AGCCTCTCCGGTAGCAAACA
Cyp1a1_1422217_a_at	TGCTCTTGCCACCTGCTGA	GGAGCACCCTGTTTGTTTCTATG
Cyp1a2_1450715_at	CCTCACTGAATGGCTTCCAC	CGATGGCCGAGTTGTTATTG
Cyp1b1_1416612_at	GCCTCAGGTGTGTTTGATGGA	AGTACAGCCCTGGTGGGAATG
Cyp7a1_1422100_at	TTCTACATGCCCTTTGGATCAG	GGACACTTGGTGTGGCTCTC
Hspa1a_1452388_at	ACCATCGAGGAGGTGGATTAGA	AGGACTTGATTGCAGGACAAAC

The "LBM" ("liver-brain mix") standard sample

A pair of samples having dissimilar gene expression profiles was chosen to evaluate the linearity of the platform. The pairs chosen were brain and liver for mouse and rat, two distinct cancer cell lines for humans, and adult liver and embryo for *Xenopus laevis*. The sample pairs were processed as described above including addition of the GSC. Two final homogenates were then blended at ratios of 100:0, 75:25, 50:50, 25:75 and 0:100 (based on cell numbers) to make five samples. These five samples were measured by Q-PCR and/or GeneChips (MG-U74v2A, MEA430A, MEA430B, MG430 2.0 (shown in Figure 1), RAE230A, HG-U95A, HG-U133, and Xenopus array).

Quantitative-PCR

Duplicate homogenate samples were treated with DNaseI (amplification grade, Invitrogen Corp., Carlsbad, CA, USA) for 15 min at room temperature, followed by SuperScript II (Invitrogen) for 50 min at 42°C for reverse transcription. Quantitative real time PCR was performed with an ABI PRISM 7900 HT sequence detection system (Applied Biosystems, Foster City, CA, USA) using SYBR Premix Ex Taq (TAKARA BIO Inc., Japan), with initial denaturation at 95°C for 10 s followed by 45 cycles of 5 s at 95°C and 60 s at 60°C, and Ct values were obtained. Primers for the genes explored in this study were selected from sequences close to the areas of Affymetrix GeneChip probe sets as shown in Table 2.

Affymetrix GeneChip measurement

The sample homogenates with GSC added were processed by the Affymetrix Standard protocol. The GeneChips used were MG-U74v2A for the uterotrophic study and Mouse 430-2 for the TCDD study (singlet measurement). The efficiency of *in vitro* transcription (IVT) was monitored by comparing the values of 5' probe sets and 3' probe sets of the control RNAs (AFFX- probe sets) including the GSC (see Quality Control below). The dose-response linearity of the five GSC spikes was checked and samples showing saturation and/or high background were re-measured from either backup tissue samples, an aliquot of homogenate, or a hybridization solution, depending on the nature of the anomaly.

Quality control

Any external spiking method, including our Percellome method, is valid for high-quality RNA samples. Therefore, the quality of the sample RNA should be carefully monitored. In addition to a common checkup by RNA electrophoresis (including capillary electrophoresis if necessary), OD ratio, and cRNA yield, we monitor the performance of IVT (*in vitro* translation) or amplification. The 3' and 5' probe set data of the spiked-in RNAs and sample RNAs (actin, GAPD and other AFFX- probe sets) that are prepared in Affymetrix GeneChip are compared to monitor the extension of RNA by the IVT process. When both the spiked-in RNAs and the sample RNAs have similar levels of 5' and 3' signals respectively, it is judged that the IVT extension was normally performed. When both spiked-in and sample RNAs have significantly lower 5' signal than 3' signal, it is judged that the IVT extension was abnormal. When only the sample RNAs showed significantly lower 5' signal than 3' signal, it is judged that the IVT extension was normal but the sample RNAs were degraded. When only the spiked-in RNAs showed significantly lower 5' signal than 3' signal, it is judged that the IVT extension was normal but the spiked-in RNAs were degraded (although we have not encountered this situation). In addition, if the degraded sample was spiked-in by the non-degraded spike RNAs and measured by GeneChip, the position of spiked-in RNAs will be offset toward abnormally higher intensity. Together, this battery of checkups considerably increases the ability to detect abnormal events that will affect the reliability of the Percellome method. When any abnormality was found, each step of sample preparation was reevaluated to regain normal data for Percellome normalization.

The web site for GeneChip data

The GeneChip data are accessible at http://www.nihs.go.jp/tox/TTG_Archive.htm.

Authors' contributions

JK drafted the concept of the Percellome method, led the project at a practical level, and drafted the manuscript. KA developed the algorithm for the Percellome calculation and wrote the calculation/visualization programs. KI developed the laboratory protocols for the Percellome procedures to the level of SOP for technicians. NN developed the Percellome Q-PCR protocol and performed the measurements, and helped in analyzing the Percellome data. AO helped develop the algorithm. YK led the animal studies. TN provided advice and led the toxicogenomics project using the Percellome method, to be approved by the Ministry of Health, Labour and Welfare of Japan.

Additional material

Additional File 1

Excel spreadsheet file containing 15 Affymetrix Mouse 430–2 GeneChip raw data of five LBM samples in triplicate (cf. Figure 1). The column name LBM-100-0-X_Signal indicates the component percentages, i.e. 100% liver 0% brain, and X = 1,2,3 indicates the triplicates. The LBM-100-0-X_Detection column indicates P for present, A for absent and M for marginal calls by Affymetrix MAS 5.0 system.

Click here for file

[http://www.biomedcentral.com/content/supplementary/1471-2164-7-64-S1.zip]

Additional File 2

Excel spreadsheet file containing Percellome data of the same LBM samples, of which raw data is listed in Additional file 1 (cf. Figure 1).

Click here for file

[http://www.biomedcentral.com/content/supplementary/1471-2164-7-64-S2.zip]

Additional File 3

Excel spreadsheet file containing 2 Affymetrix MG-U74v2 raw data of a blank sample with the GSC (horizontal axis of Figure 2a) and blank with the five spike RNAs at a high dosage (vertical axis of Figure 2a).

Click here for file

[http://www.biomedcentral.com/content/supplementary/1471-2164-7-64-S3.zip]

Additional File 4

Excel spreadsheet file containing 2 Affymetrix MG-U74v2 raw data of a liver sample with GSC (horizontal axis of Figure 2b) and without GSC (vertical axis of Figure 2b).

Click here for file

[http://www.biomedcentral.com/content/supplementary/1471-2164-7-64-S4.zip]

Additional File 5

(first quarter of a data set consisting of 2 hr, 4 hr, 8 hr, and 24 hr data, divided because of the upload file size limitation)]: an Excel spreadsheet file containing 2 hr data (15 GeneChip data) of the total of 60 Affymetrix Mouse 430-2 GeneChip raw data of the TCDD study consisting of 20 different treatment groups in triplicate (cf. Figure 5). The column name DoseXXX-TimeYY-Z_Signal indicates the dosage and sampling time after TCDD administration in hours, e.g. XXX = 001 indicates 1 microgram/kg group, YY = 02 indicates two hours after administration, and Z = 1,2,3 indicates animal triplicate. The DoseXXX-TimeYY-Z_Detection column indicates P for present, A for absent and M for marginal calls by Affymetrix MAS 5.0 system.

Click here for file

[http://www.biomedcentral.com/content/supplementary/1471-2164-7-64-S5.zip]

Additional File 6

(second quarter of a data set consisting of 2 hr, 4 hr, 8 hr, and 24 hr data, divided because of the upload file size limitation)]: an Excel spreadsheet file containing 4 hr data (15 GeneChip data) of the total of 60 Affymetrix Mouse 430-2 GeneChip raw data of the TCDD study consisting of 20 different treatment groups in triplicate (cf. Figure 5). The column name DoseXXX-TimeYY-Z_Signal indicates the dosage and sampling time after TCDD administration in hours, e.g. XXX = 001 indicates 1 microgram/kg group, YY = 02 indicates two hours after administration, and Z = 1,2,3 indicates animal triplicate. The DoseXXX-TimeYY-Z_Detection column indicates P for present, A for absent and M for marginal calls by Affymetrix MAS 5.0 system.

Click here for file

[http://www.biomedcentral.com/content/supplementary/1471-2164-7-64-S6.zip]

Additional File 7

(third quarter of a data set consisting of 2 hr, 4 hr, 8 hr, and 24 hr data, divided because of the upload file size limitation)]: an Excel spreadsheet file containing 8 hr data (15 GeneChip data) of the total of 60 Affymetrix Mouse 430-2 GeneChip raw data of the TCDD study consisting of 20 different treatment groups in triplicate (cf. Figure 5). The column name DoseXXX-TimeYY-Z_Signal indicates the dosage and sampling time after TCDD administration in hours, e.g. XXX = 001 indicates 1 microgram/kg group, YY = 02 indicates two hours after administration, and Z = 1,2,3 indicates animal triplicate. The DoseXXX-TimeYY-Z_Detection column indicates P for present, A for absent and M for marginal calls by Affymetrix MAS 5.0 system.

Click here for file

[http://www.biomedcentral.com/content/supplementary/1471-2164-7-64-S7.zip]

Additional File 8

(last quarter of a data set consisting of 2 hr, 4 hr, 8 hr, and 24 hr data, divided because of the upload file size limitation)]: an Excel spreadsheet file containing 24 hr data (15 GeneChip data) of the total of 60 Affymetrix Mouse 430-2 GeneChip raw data of the TCDD study consisting of 20 different treatment groups in triplicate (cf. Figure 5). The column name DoseXXX-TimeYY-Z_Signal indicates the dosage and sampling time after TCDD administration in hours, e.g. XXX = 001 indicates 1 microgram/kg group, YY = 02 indicates two hours after administration, and Z = 1,2,3 indicates animal triplicate. The DoseXXX-TimeYY-Z_Detection column indicates P for present, A for absent and M for marginal calls by Affymetrix MAS 5.0 system.

Click here for file

[http://www.biomedcentral.com/content/supplementary/1471-2164-7-64-S8.zip]

Additional File 9

(first quarter of a data set consisting of 2 hr, 4 hr, 8 hr, and 24 hr data, divided because of the upload file size limitation)]: an Excel spreadsheet file containing 2 hr Percellome data (15 sample data) of the 60 samples of the TCDD study (cf. Figure 5), of which corresponding raw data is listed in Additional file 5.
Click here for file
[http://www.biomedcentral.com/content/supplementary/1471-2164-7-64-S9.zip]

Additional File 10

(second quarter of a data set consisting of 2 hr, 4 hr, 8 hr, and 24 hr data, divided because of the upload file size limitation)]: an Excel spreadsheet file containing 4 hr Percellome data (15 sample data) of the 60 samples of the TCDD study (cf. Figure 5), of which corresponding raw data is listed in Additional file 6.
Click here for file
[http://www.biomedcentral.com/content/supplementary/1471-2164-7-64-S10.zip]

Additional File 11

(third quarter of a data set consisting of 2 hr, 4 hr, 8 hr, and 24 hr data, divided because of the upload file size limitation)]: an Excel spreadsheet file containing 8 hr Percellome data (15 sample data) of the 60 samples of the TCDD study (cf. Figure 5), of which corresponding raw data is listed in Additional file 7.
Click here for file
[http://www.biomedcentral.com/content/supplementary/1471-2164-7-64-S11.zip]

Additional File 12

(last quarter of a data set consisting of 2 hr, 4 hr, 8 hr, and 24 hr data, divided because of the upload file size limitation)]: an Excel spreadsheet file containing 24 hr Percellome data (15 sample data) of the 60 samples of the TCDD study (cf. Figure 5), of which corresponding raw data is listed in Additional file 8.
Click here for file
[http://www.biomedcentral.com/content/supplementary/1471-2164-7-64-S12.zip]

Additional File 13

Excel spreadsheet file containing 15 Affymetrix MG-U74v2 A GeneChip raw data of the uterotrophic response study (cf. Figure 6). The column name X-Y_Signal indicates the treatment (V = vehicle, Low = low dose, etc) and animal triplicate (Y = 1,2,3). The X-Y_Detection column indicates P for present, A for absent and M for marginal calls by Affymetrix MAS 5.0 system.
Click here for file
[http://www.biomedcentral.com/content/supplementary/1471-2164-7-64-S13.zip]

Additional File 14

Excel spreadsheet file containing Percellome data of the same 15 samples of the uterotrophic response study (cf. Figure 6), of which raw data is listed in Additional file 13.
Click here for file
[http://www.biomedcentral.com/content/supplementary/1471-2164-7-64-S14.zip]

Acknowledgements

The authors thank Tomoko Ando, Noriko Moriyama, Yuko Kondo, Yuko Nakamura, Maki Abe, Nae Matsuda, Kenta Yoshiki, Ayako Imai, Koichi Morita, Hisako Aihara and Chiyuri Aoyagi for technical support, and Dr. Bruce Blumberg and Dr. Thomas Knudson for critical reading of the manuscript. This study was supported by Health Sciences Research Grants H13-Seikatsu-012, H13-Seikatsu-013, H14-Toxico-001 and H15-Kagaku-002 from the Ministry of Health, Labour and Welfare, Japan.

References

1. Holstege FC, Jennings EG, Wyrick JJ, Lee TI, Hengartner CJ, Green MR, Golub TR, Lander ES, Young RA: **Dissecting the regulatory circuitry of a eukaryotic genome.** *Cell* 1998, **95:**717-728.
2. Hill AA, Brown EL, Whitley MZ, Tucker-Kellogg G, Hunter CP, Slonim DK: **Evaluation of normalization procedures for oligonucleotide array data based on spiked cRNA controls.** *Genome Biol* 2001, **2:**. RESEARCH0055
3. Lee PD, Sladek R, Greenwood CM, Hudson TJ: **Control genes and variability: absence of ubiquitous reference transcripts in diverse mammalian expression studies.** *Genome Res* 2002, **12:**292-297.
4. van de Peppel J, Kemmeren P, van Bakel H, Radonjic M, van Leenen D, Holstege FC: **Monitoring global messenger RNA changes in externally controlled microarray experiments.** *EMBO Rep* 2003, **4:**387-393.
5. Yang YH, Dudoit S, Luu P, Lin DM, Peng W, Ngai J, Speed TP: **Normalization for cDNA microarray data: a robust composite method addressing single and multiple slide systematic variation.** *Nucleic Acids Res* 2002, **30:**e15.
6. Hekstra D, Taussig AR, Magnasco M, Naef F: **Absolute mRNA concentrations from sequence-specific calibration of oligonucleotide arrays.** *Nucleic Acids Res* 2003, **31:**1962-1968.
7. Sterrenburg E, Turk R, Boer JM, van Ommen GB, den Dunnen JT: **A common reference for cDNA microarray hybridizations.** *Nucleic Acids Res* 2002, **30:**e116.
8. Dudley AM, Aach J, Steffen MA, Church GM: **Measuring absolute expression with microarrays with a calibrated reference sample and an extended signal intensity range.** *Proc Natl Acad Sci USA* 2002, **99:**7554-7559.
9. Talaat AM, Howard ST, Hale W, Lyons R, Gamer H, Johnston ST: **Genomic DNA standards for gene expression profiling in Mycobacterium tuberculosis.** *Nucleic Acids Res* 2002, **30:**e104.
10. Bolstad BM, Irizarry RA, Astrand M, Speed TP: **A comparison of normalization methods for high density oligonucleotide array data based on variance and bias.** *Bioinformatics* 2003, **19:**185-193.
11. Lockhart DJ, Dong H, Byrne MC, Follettie MT, Gallo MV, Chee MS, Mittmann M, Wang C, Kobayashi M, Horton H, Brown EL: **Expression monitoring by hybridization to high-density oligonucleotide arrays.** *Nat-Biotechnol* 1996, **14:**1675-1680.
12. Kanno J, Onyon L, Peddada S, Ashby J, Jacob E, Owens W: **The OECD program to validate the rat uterotrophic bioassay. Phase 2: dose-response studies.** *Environ Health Perspect* 2003, **111:**1530-1549.
13. Kanno J: **Reverse toxicology as a future predictive toxicology.** In *Toxicogenomics* Edited by: Inoue T, Pennie ED. Tokyo, Springer-Verlag; 2002:213-218.

0888-8809/06/$15.00/0
Printed in U.S.A.

Molecular Endocrinology 20(9):2141–2155

doi: 10.1210/me.2005-0367

Endocrine-Disrupting Organotin Compounds Are Potent Inducers of Adipogenesis in Vertebrates

Felix Grün, Hajime Watanabe, Zamaneh Zamanian, Lauren Maeda, Kayo Arima, Ryan Cubacha, David M. Gardiner, Jun Kanno, Taisen Iguchi, and Bruce Blumberg

Department of Developmental and Cell Biology (F.G., Z.Z., L.M., K.A., R.C., D.M.G., B.B.), University of California Irvine, Irvine California 92697-2300; National Institutes of Natural Sciences (H.W., T.I.), National Institute for Basic Biology, Okazaki Institute for Integrative Bioscience, Okazaki 444-8787, Japan; and Division of Cellular & Molecular Toxicology (J.K.), Biological Safety Research Center, National Institute of Health Sciences, Setagaya-ku, Tokyo 158-8501, Japan

Dietary and xenobiotic compounds can disrupt endocrine signaling, particularly of steroid receptors and sexual differentiation. Evidence is also mounting that implicates environmental agents in the growing epidemic of obesity. Despite a long-standing interest in such compounds, their identity has remained elusive. Here we show that the persistent and ubiquitous environmental contaminant, tributyltin chloride (TBT), induces the differentiation of adipocytes *in vitro* and increases adipose mass *in vivo*. TBT is a dual, nanomolar affinity ligand for both the retinoid X receptor (RXR) and the peroxisome proliferator-activated receptor γ (PPARγ). TBT promotes adipogenesis in the murine 3T3-L1 cell model and perturbs key regulators of adipogenesis and lipogenic pathways *in vivo*. Moreover, *in utero* exposure to TBT leads to strikingly elevated lipid accumulation in adipose depots, liver, and testis of neonate mice and results in increased epididymal adipose mass in adults. In the amphibian *Xenopus laevis*, ectopic adipocytes form in and around gonadal tissues after organotin, RXR, or PPARγ ligand exposure. TBT represents, to our knowledge, the first example of an environmental endocrine disrupter that promotes adipogenesis through RXR and PPARγ activation. Developmental or chronic lifetime exposure to organotins may therefore act as a chemical stressor for obesity and related disorders. (*Molecular Endocrinology* 20: 2141–2155, 2006)

ORGANOTINS ARE A diverse group of widely distributed environmental pollutants. Tributyltin chloride (TBT) and bis(triphenyltin) oxide (TPTO), have pleiotropic adverse effects on both invertebrate and vertebrate endocrine systems. Organotins were first used in the 1960s as antifouling agents in marine shipping paints, although such use has been restricted in recent years. Organotins persist as prevalent contaminants in dietary sources, such as fish and shellfish, and through pesticide use on high-value food crops (1, 2). Additional human exposure to organotins may occur through their use as antifungal agents in wood treatments, industrial water systems, and textiles. Mono- and diorganotins are prevalently used as stabilizers in the manufacture of polyolefin plastics (polyvinyl chloride), which introduces the potential for transfer by contact with drinking water and foods.

Exposure to organotins such as TBT and TPTO results in imposex, the abnormal induction of male sex characteristics in female gastropod mollusks (3, 4). Bioaccumulation of organotins decreases aromatase activity leading to a rise in testosterone levels that promotes development of male characteristics (5). Imposex results in impaired reproductive fitness or sterility in the affected animals and is one of the clearest examples of environmental endocrine disruption. TBT exposure also leads to masculinization of at least two fish species (6, 7), but TBT is only reported to have modest adverse effects on mammalian male and female reproductive tracts and does not alter sex ratios (8, 9). Instead, hepatic-, neuro-, and immunotoxicity appear to be the predominant effects of organotin exposure (10). Hence, the current mechanistic understanding of the endocrine-disrupting potential of organotins is based on their direct actions on the levels or activity of key steroid-regulatory enzymes such as aromatase and more general toxicity mediated via damage to mitochondrial functions and subsequent cellular stress responses (11–15).

However, it remains an open question whether *in vivo* organotins act primarily as protein and enzyme

First Published Online April 13, 2006

Abbreviations: Acac, Acetyl-coenzyme A carboxylase; b.w., body weight; C/EBP, CCAAT/enhancer binding protein; 9-*cis* RA, 9-cis retinoic acid; DMSO, dimethylsulfoxide; F, forward; Fatp, fatty acid transport protein; LBD, ligand-binding domain; LXR, liver X receptor; MDIT, 3-isobutyl-1-methylxanthine, dexamethasone, insulin and T_3 adipocyte differentiation mix; PPAR, peroxisome proliferator-activated receptor; R, reverse; RAR, retinoic acid receptor; RXR, retinoid X receptor; Srebf1, sterol-regulatory element binding factor 1; TBT, tributyltin chloride; TPTO, triphenyltin oxide; TTNPB, (E)-4-[2-(5,6,7,8-tetrahydro-5,5,8,8-tetramethyl-2-naphthylenyl)-1-propenyl] benzoic acid; VDR, vitamin D receptor.

***Molecular Endocrinology* is published monthly by The Endocrine Society (http://www.endo-society.org), the foremost professional society serving the endocrine community.**

inhibitors, or rather mediate their endocrine-disrupting effects at the transcriptional level. Recent work has shown that aromatase mRNA levels can be down-regulated in human ovarian granulosa cells by treatment with organotins or ligands for the nuclear hormone receptors, retinoid X receptor (RXRs) or peroxisome proliferator-activated receptor γ (PPARγ) (16–18). Furthermore, Nishikawa *et al.* (19) have demonstrated that the gastropod *Thais clavigara* RXR homolog is responsive to 9-cis-retinoic acid (9-*cis*-RA) and TBT, and 9-*cis* RA can also induce imposex, suggesting a conserved transcriptional mechanism for TBT action across phyla. These ligand-dependent transcription factors belong to the nuclear hormone receptor superfamily—a group of approximately 150 members (48 human genes) that includes the estrogen receptor, androgen receptor, glucocorticoid receptor, thyroid hormone receptor, vitamin D receptor (VDR), retinoic acid receptors (RARs and RXRs), PPARs, and numerous orphan receptors. We were therefore intrigued by the similar effects of TBT and RXR/PPARγ ligands on mammalian aromatase mRNA expression and hypothesized that TBT might be exerting some of its biological effects via transcriptional regulation of gene expression through activation of one or more nuclear hormone receptors.

Our results show that organotins such as TBT are indeed potent and efficacious agonistic ligands of the vertebrate nuclear receptors, retinoid X receptors (RXRs) and PPARγ. The physiological consequences of receptor activation predict that permissive RXR heterodimer target genes and downstream signaling cascades are sensitive to organotin misregulation. Consistent with this prediction we observe that organotins phenocopy the effects of RXR and PPARγ ligands using *in vitro* and *in vivo* models of adipogenesis. Therefore, TBT and related organotin compounds are the first of a potentially new class of environmental endocrine disrupters that targets adipogenesis by modulating the activity of key regulatory transcription factors in the adipogenic pathway, RXRα and PPARγ. The existence of such xenobiotic compounds was previously hypothesized (20, 21). Our results suggest that developmental exposure to TBT and its congeners that activate RXR/PPARγ might be expected to increase the incidence of obesity in exposed individuals and that chronic lifetime exposure could act as a potential chemical stressor for obesity and obesity-related disorders.

RESULTS

Organotins Are Agonists of Vertebrate RXR and RXR-Permissive Heterodimers

Many known or suspected environmental endocrine-disrupting chemicals mimic natural lipophilic hormones that act through members of the superfamily of nuclear receptor transcription factors (22, 23). In a screen of high-priority endocrine-disrupting chemicals against a bank of vertebrate nuclear receptor ligand-binding domains (LBDs), we observed that organotins, specifically tributyltin chloride (TBT) and bis(triphenyltin) oxide (TPTO), could fully activate an RXRα LBD construct (GAL4-RXRα) in transient transfection assays. Both TBT and TPTO were as potent (EC_{50} ~3–10 nM) as 9-*cis* retinoic acid, an endogenous RXR ligand and approximately 2- to 5-fold less potent than the synthetic RXR-specific ligands LG100268 (EC_{50} ~ 2 nM) or AGN195203 (EC_{50} ~ 0.5 nM) (Fig. 1A and see Table 2). Maximal activation for TBT reached the same levels as LG100268 or AGN195203.

We next tested whether activation by TBT was unique to RXRα only, restricted to RXR heterodimer complexes, or a general nuclear receptor transcriptional response (Fig. 1, B–D, and Table 1). TBT activated RXRα and RXRγ from the amphibian *Xenopus laevis* in addition to human RXRs (Table 1). Our results are consistent with recent findings by Nishikawa *et al.* (19, 24) that organotins promote activation of all three human RXR subtypes in a yeast two-hybrid screen. We also observed significant activation of receptors typically considered to be permissive heterodimeric partners of RXR including human PPARγ (Fig. 1B, ~30% maximal activation of 10 μM troglitazone, but note that activation is compromised by cellular toxicity above 100 nM), PPARδ, liver X receptor (LXR), and the orphan receptor NURR1. In contrast, typical nonpermissive partners such as RARs, thyroid hormone receptor, and VDR failed to show activation by organotins (Fig. 1C and Table 1). Murine PPARα was also not activated by TBT although it was fully activated by its specific synthetic agonist WY-14643 (Fig. 1D). The steroid and xenobiotic receptor was likewise unresponsive. The orphan receptor NURR1, which has no discernable ligand pocket and is believed to be ligand independent (25), was nevertheless activated 7- to 10-fold at 100 nM TBT. Similarly, other RXR-specific ligands, *e.g.* LG100268, activated NURR1 to the same degree, suggesting that this response occurred through NURR1's heterodimeric partner RXR as has been previously described (25, 26). Like other RXR-specific ligands, tributyltin was also able to promote the ligand-dependent recruitment of nuclear receptor cofactors such as receptor-associated coactivator 3 (ACTR), steroid receptor coactivator-1, and PPAR-binding protein in mammalian two-hybrid interaction assays (data not shown). We infer from these results that nuclear receptor activation by TBT activation is specific to a small subset of receptors and not a consequence of a general effect on the cellular transcriptional machinery.

We next investigated the relationship between the structure of the tin compounds and RXR activation by testing the response of GAL4-RXRα to mono-, di-, tri-, and tetra-substituted butyltin, branched side chains, variations in the alkyl chain length, and changes in the halide component (Fig. 1A and Table 2). Overall, trialkyltin compounds were the most effective with nano-

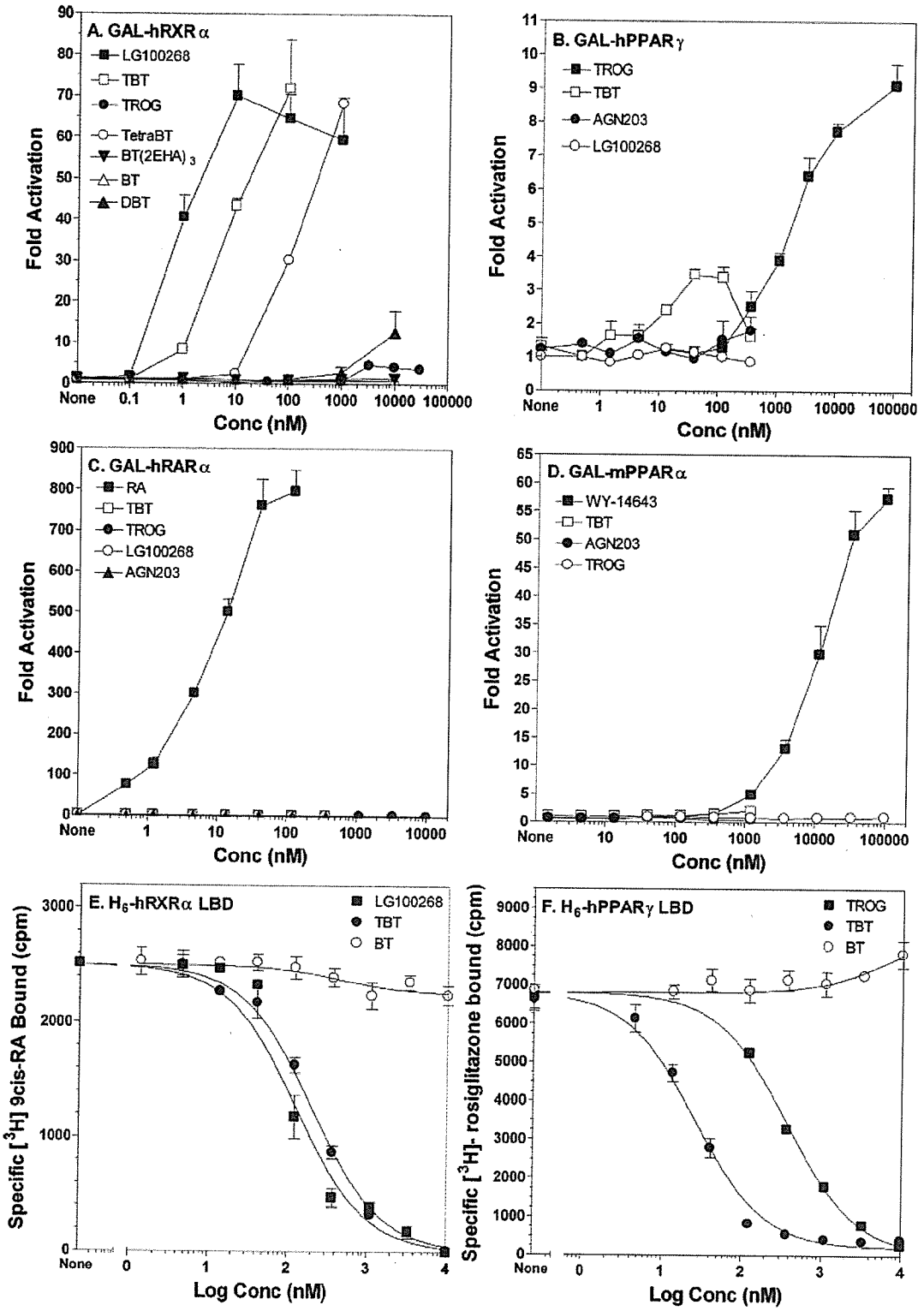

Fig. 1. Organotins Are Agonist Ligands of RXRα and PPARγ

Organotins are high-affinity ligand agonists of RXRα and PPARγ. A–D, Activation of GAL4-hRXRα, -hPPARγ, -hRARα, or -hPPARα in transiently transfected Cos7 cells by organotins and receptor-specific ligands. Data represent reporter luciferase activity normalized to β-galactosidase and plotted as the average fold activation ± SEM (n = 3) relative to solvent-only controls from representative experiments. E and F, Competition binding curves of histidine-tagged RXRα or PPARγ LBDs with TBT. Data shown are from a representative experiment analyzed in GraphPad Prism 4.0 and K_i values deduced (Table 3). Conc, Concentration; DBT, dibutyltin chloride; TROG, troglitazone.

Table 1. TBT Activates RXRs and RXR-Permissive Heterodimers

GAL4-NR LBD	Fold Activation at 60 nM TBT	Permissive RXR Heterodimer
RXRα (*Homo sapiens*)	60	Yes
RXRα (*X. laevis*)	25	Yes
RXRγ (*X. laevis*)	7.0	Yes
NURR1 (*H. sapiens*)	7.0	Yes
LXR (*H. sapiens*)	2.1	Yes
PPARα (*Mus musculus*)	0.7	Yes
PPARγ (*H. sapiens*)	5.3	Yes
PPARδ (*H. sapiens*)	1.7	Yes
RARα (*H. sapiens*)	0.7	No
TR&β (*H. sapiens*)	0.4	No
VDR (*H. sapiens*)	0.5	No
SXR (*H. sapiens*)	1.0	No

Data are fold activation at 60 nM TBT relative to solvent-only controls of transiently transfected Cos7 cells after 24 h ligand treatment. SXR, Steroid and xenobiotic receptor; TR, thyroid hormone receptor.

molar EC_{50} values. Monobutyltin gave no significant activation whereas dibutyltin was moderately active in the micromolar range (Fig. 1A and Table 2). Tetrabutyltin was 20-fold less potent than TBT, whereas the branched side-chain butyltin tris(2-ethylhexanoate) [BT(2-EHA)$_3$] was inactive (Table 2). Although activation by dialkyltins is weaker than that of TBT, it is potentially significant due to their widespread use in the manufacture of polyvinyl chloride plastics and greater solubility than TBT.

The effect of the hydrocarbon chain length was very pronounced, suggesting an important structure-activity relationship. A reduction in hydrophobicity from butyl to ethyl side chains raised the EC_{50} value by almost 1000-fold into the micromolar range. Trimethyltin was weakly active only above 100 μM (Table 2). Substitution of the halide component had no significant effect on the EC_{50} values for TBT, probably due to the lability of the halide atom through exchange in aqueous tissue culture media where chloride ions are prevalent.

Table 2. Organotin EC_{50} Values for Nuclear Receptor LBDs

Ligand	GAL4-NR LBD Transactivation (EC_{50} Values, nM)		
	hRXRα	hRARα	hPPARγ
LGD268	2–5	na	na
AGN195203	0.5–2	na	na
9-*cis* RA	15	na	na
all-*trans* RA	na	8	na
Butyltin chloride	na	na	na
Dibutyltin chloride	3000	na	na
TBT	3–8	na	20
Tetrabutyltin	150	ND	ND
Di(triphenyltin)oxide	2–10	na	20
Butyltin tris(2-ethylhexanoate)	na	ND	ND
Troglitazone	na	na	1000
Tributyltin fluoride	3	ND	ND
Tributyltin bromide	4	ND	ND
Tributyltin iodide	4	ND	ND
Triethyltin bromide	2800	ND	ND
Trimethyltin chloride	>10000	ND	ND

na, Not active; ND, not determined. EC_{50} values were determined from dose-response curves of GAL4-NR LBD construct activation in transiently transfected Cos7 cells after 24-h ligand exposure.

TBT Is a Potent Ligand of Both RXRα and PPARγ

Many, if not most, natural and synthetic nuclear receptor agonists act as ligands that specifically interact with their cognate receptor LBDs. We therefore performed equilibrium competition binding experiments with purified histidine-tagged human RXRα (H_6-RXRα) and PPARγ (H_6-PPARγ) LBDs to determine whether the potent and specific activation of these receptors by TBT was due to direct ligand-receptor interaction (Fig. 1, E and F).

The equilibrium binding curves indicate that TBT is a high-affinity, competitive ligand for 9-*cis* RA-bound RXRα. The inhibition equilibrium dissociation constant was calculated by the Chang-Prusoff method [inhibition constant (K_i) = dissociation constant (K_d)] as 12.5 nM (10–15 nM; 95% confidence interval) (Table 3). By comparison, the value obtained for the synthetic RXR agonist LG100268 was 7.5 nM, which compared favorably with its published value of approximately 3 ± 1 nM (27). Therefore, the identification of TBT as an RXR ligand expands the molecular definition of known rexinoids (agonists able to activate RXR) to include this structurally unique class of organotin compounds.

Somewhat surprisingly, we also observed potent specific competitive binding by TBT for rosiglitazone bound to human PPARγ LBD (Fig. 2B). The deduced K_i of 20 nM (17–40 nM; 95% confidence interval) was slightly higher than for RXRα but significantly better than the K_i for the PPARγ agonist troglitazone, which

Table 3. TBT Binding Constants (K_d) for hRXRα and hPPARγ LBDs

Ligand	Receptor Competitive Inhibition Binding Constants K_i (nM ± 95% CI)		
	H_6-RXRα	H_6-PPARγ	Published
TBT	12.5 (10–15)	20 (17–40)	
LG100268	7.5 (6–10)	ND	3 ± 1[a]
Troglitazone	ND	300 (270–335)	300 ± 30[b]

Competition binding curves were determined at constant ^{3}H-specific ligand concentrations [20 nM 9-*cis*-RA, K_d = 1.4 nM (87) or rosiglitazone, K_d = 41 nM (88)] with increasing cold competitor ligands over the range indicated in Fig. 1, E and F. Data were analyzed in GraphPad Prism by nonlinear regression of a competitive one-site binding equation (Chang-Prusoff method) to determine K_i values ± 95% confidence intervals (n = 3). CI, Confidence interval; ND, not determined.
[a] RXRα:LG100268 K_d = 3 ± 1 nM (27).
[b] PPARγ:troglitazone K_d = 300 ± 30 nM (28).

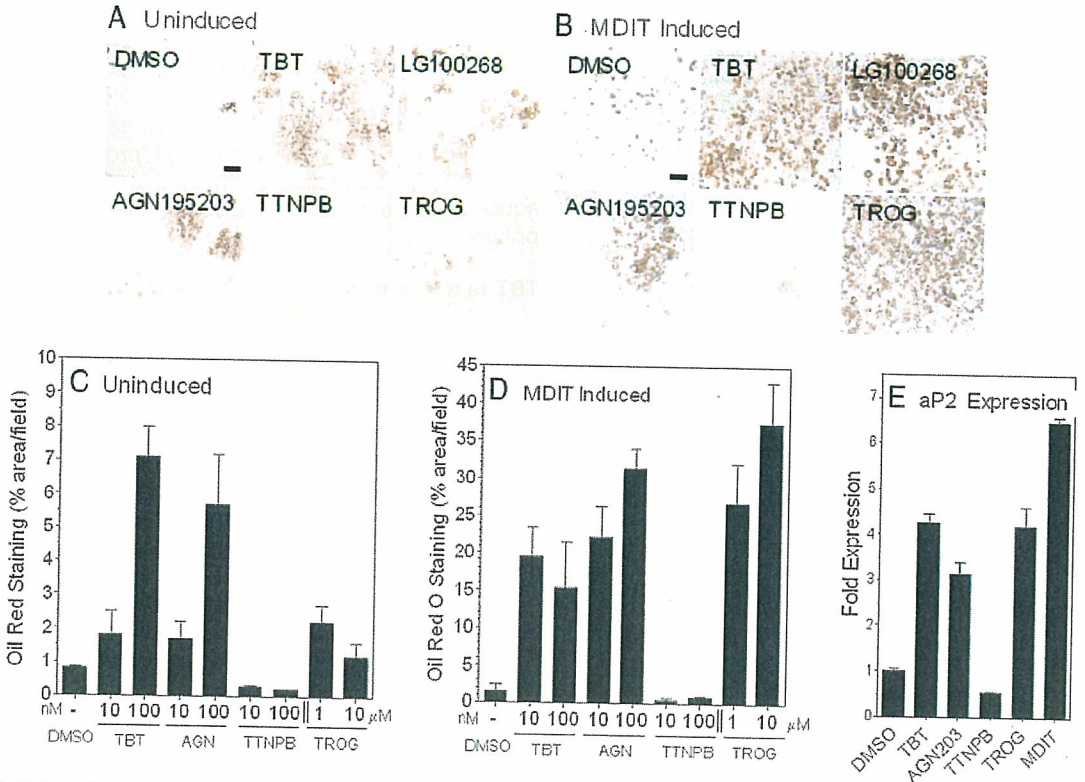

Fig. 2. Tributyltin Induces Adipogenesis in 3T3-L1 Cells

Uninduced (A) and MDIT-induced (B) 3T3-L1 cultures grown for 1 wk in the presence of vehicle (DMSO), or ligands were analyzed for mature adipocyte differentiation by Oil Red O staining. *Scale bar* represents 100 μm. C and D, The percentage area stained was determined by automated analysis of random fields (n = 9) from high-contrast dissecting scope photographs of monolayers analyzed in ImageJ; 1–100 nM of TBT, AGN195203, and TTNPB or 1–10 μM troglitazone. E, Quantitative real-time PCR (QRT-PCR) of adipocyte-specific fatty acid binding protein aP2 (aP2/Fabp4) expression levels in postconfluent 3T3-L1 cells treated with the indicated ligands for 24 h. Data were normalized to glyceraldehyde-3-phosphate dehydrogenase controls and plotted as average fold induction ± SEM (n = 3).TROG, Troglitazone.

yielded a K_i of 300 nM, consistent with its published K_d (28). The K_d values for TBT binding to RXRα (12.5 nM) and PPARγ (20 nM) are also in close agreement with EC_{50} values obtained from transient transfection assays using GAL4-RXRα and GAL4-PPARγ constructs (Table 2).

Taken together, these data show that organotins such as TBT, although structurally distinct from previously described natural or synthetic ligands, can interact with RXRα and PPARγ, via direct ligand binding to induce productive receptor-coactivator interactions and promote transcription in a concentration-dependent manner. Organotins are therefore potent nanomolar receptor activators on par with synthetic RXR and PPARγ ligands such as LG100268, AGN195203, and thiazolidinediones.

TBT Promotes Adipogenesis in the Murine 3T3-L1 Cell (Embryonic Murine Preadipocyte Fibroblast Cell Line) Model

Numerous studies have demonstrated the critical role played by RXRα:PPARγ signaling in regulation of mammalian adipogenesis (29–31). In the murine 3T3-L1 preadipocyte cell model, adipogenic signals induce early key transcriptional regulators such as CCAAT/enhancer binding proteins (C/EBPs) β and δ that lead to mitotic clonal expansion of growth-arrested preadipocytes and induction of the late differentiation factors C/EBPα and PPARγ (32–34). The combination of C/EBPα expression together with PPARγ signaling efficiently drives terminal adipocyte differentiation and lipid accumulation. We therefore tested whether TBT signaling through RXR:PPARγ could promote adipogenesis in the murine 3T3-L1 differentiation assay and compared its effect to other RXR-specific or PPARγ ligands (Fig. 2). Undifferentiated 3T3-L1 cells were cultured for 1 wk in the presence of ligands either with or without a prior 2-d treatment with MDIT (an adipogenic-sensitizing cocktail of 3-isobutyl-1-methylxanthine, dexamethasone, insulin, and T_3) (35). Cells were then scored for lipid accumulation using Oil Red O staining to determine the degree of terminal adipocyte differentiation. TBT was as effective as LG100268 or AGN195203 in promoting dif-

ferentiation in the absence of MDIT treatment, increasing the number of differentiated adipocytes about 7-fold over solvent-only controls (Fig. 2, A and C). The PPARγ agonist troglitazone was a weak inducer in the absence of MDIT. Prior treatment with MDIT increased the response to TBT, LG100268, and AGN195203 a further 3- to 5-fold (Fig. 2, B and D). MDIT treatment also boosted the response to troglitazone to equivalent levels as expected from published studies showing that combination treatment with PPARγ ligands promotes efficient adipocyte differentiation (36–38). In contrast, the RAR agonist TTNPB inhibited the differentiation of 3T3-L1 cells, consistent with previously published data that showed RAR signaling blocks adipogenesis during the early stages of differentiation *in vitro* and can modulate adiposity and whole body weight *in vivo* (39–41). The differential response of 3T3-L1 cells to receptor-selective retinoids indicates that TBT favors RXR homodimer or permissive RXR-heterodimer rather than RXR:RAR signaling in this cell model.

Adipocyte differentiation by TBT was accompanied by direct transcriptional effects on RXR:PPARγ targets such as adipocyte-specific fatty acid-binding protein (aP2) mRNA. The aP2 promoter contains response elements sensitive to C/EBP factors and RXRα:PPARγ signaling (42). Quantitative real-time PCR analysis showed aP2 levels were elevated by TBT treatment approximately 5-fold at 24 h (Fig. 2E) and 45-fold at 72 h (data not shown). LG100268, troglitazone, and MDIT treatment also increased aP2 expression at these time points whereas the RAR agonist TTNPB was inhibitory, consistent with the observed cellular responses.

TBT Induces Adipogenic Regulators and Markers of RXRα:PPARγ Signaling *in Vivo*

The ability of organotins to regulate RXRα:PPARγ target genes and key modulators of adipogenesis and lipid homeostasis *in vivo* has not been previously examined. Therefore, we next asked whether TBT could perturb expression of critical transcriptional mediators of adipogenesis such as RXRα, PPARγ, C/EBPα/β/δ, and sterol regulatory element binding factor 1 (Srebf1) as well as known target genes of RXRα:PPARγ signaling from liver, epididymal adipose tissue, and testis of 6-wk-old male mice dosed for 24 h with TBT [0.3 mg/kg body weight (b.w.)], AGN195203 (0.3 mg/kg b.w.), troglitazone (3 mg/kg b.w), or vehicle (corn oil) administered by ip injection. TBT either had no effect or weakly repressed RXRα and PPARγ transcription in liver (Fig. 3, A and B). A more pronounced decrease was observed for RXRα, PPARγ, C/EBPα, and C/EBPδ in adipose tissue and testis (Fig. 3, B and C). In contrast, TBT, AGN195203, and troglitazone significantly induced expression of the early adipogenic transcription factor C/EBPβ in liver and testis, whereas it was more weakly induced in adipose tissue. Induction was strongest in testis where TBT and troglitazone increased expression greater than 10-fold and AGN195203 increased expression 60-fold compared with vehicle controls (Fig. 3C). In addition to C/EBPβ, the proadipogenic transcription factor Srebf1 was also significantly increased in adipose tissue by all three receptor ligands and weakly induced in liver.

We also observed coordinate changes in several well-characterized direct target genes of RXR:PPARγ signaling. Fatty acid transport protein (Fatp) acts as a key control point for regulation of cellular fatty acid content. The Fatp promoter contains a functional PPAR response element shown to be sensitive to RXR:PPARγ signaling in 3T3-L1 adipocytes and white fat (43–46). Fatp mRNA levels were up regulated 2- to 3-fold in liver and epididymal adipose tissue but not testis by TBT, AGN195203, and troglitazone (see Fig. 5, A and B). Similarly, the PPARγ target phosphoenolpyruvate carboxykinase 1 (PEPCK/Pck1) (47), the rate-limiting step in hepatic gluconeogenesis and adipose glyceroneogenesis, was up-regulated in liver and adipose tissues by TBT or troglitazone treatment.

Signaling through RXR:PPARγ, RXR:LXR, and ADD1/Srebf1 in hepatocytes has been shown to modulate fatty acid synthesis through transcriptional control of acetyl-coenzyme A carboxylase (Acac), the rate-limiting step in long-chain fatty acid synthesis (48, 49), as well as fatty acid synthase (Fasn) (50–53). Hepatic expression of both Acac and Fasn was unregulated between 1.5–2.5-fold by TBT, AGN195203, and troglitazone. Therefore, the coordinate increased expression of Fatp, Pck1, Acac, and Fasn in liver suggests that TBT stimulates fatty acid uptake and triglyceride synthesis. Similar changes have been reported in the induction of hepatic steatosis by overactive PPARγ signaling (49, 54).

Taken together, these data show that TBT exposure induces lipogenic RXR:PPARγ target gene expression, in adipose tissue and liver, and modulates associated early adipocyte differentiation factors such as C/EBPβ and Srebf1. We inferred from these data that organotins are potential adipogenic agents *in vivo*.

Developmental Exposure to TBT Disrupts Lipid Homeostasis and Adipogenesis in Vertebrates

Based on its molecular pharmacology, ability to induce 3T3-L1 adipocyte differentiation, and *in vivo* transcriptional responses, we reasoned that TBT would disrupt normal endocrine control over lipid homeostasis and impact adipogenesis, particularly when exposure occurred during sensitive periods of development. We therefore tested this hypothesis in two vertebrate model systems, mouse and *X. laevis*, during embryogenesis.

Pregnant C57BL/6 mice were injected daily from gestational d 12–18 with TBT (0.05 or 0.5 mg/kg body weight ip) dissolved in sesame oil or vehicle alone. Pups were then killed at birth, and histological sections were prepared from liver, testis, mammary gland, and inguinal adipose tissue. Sections were stained

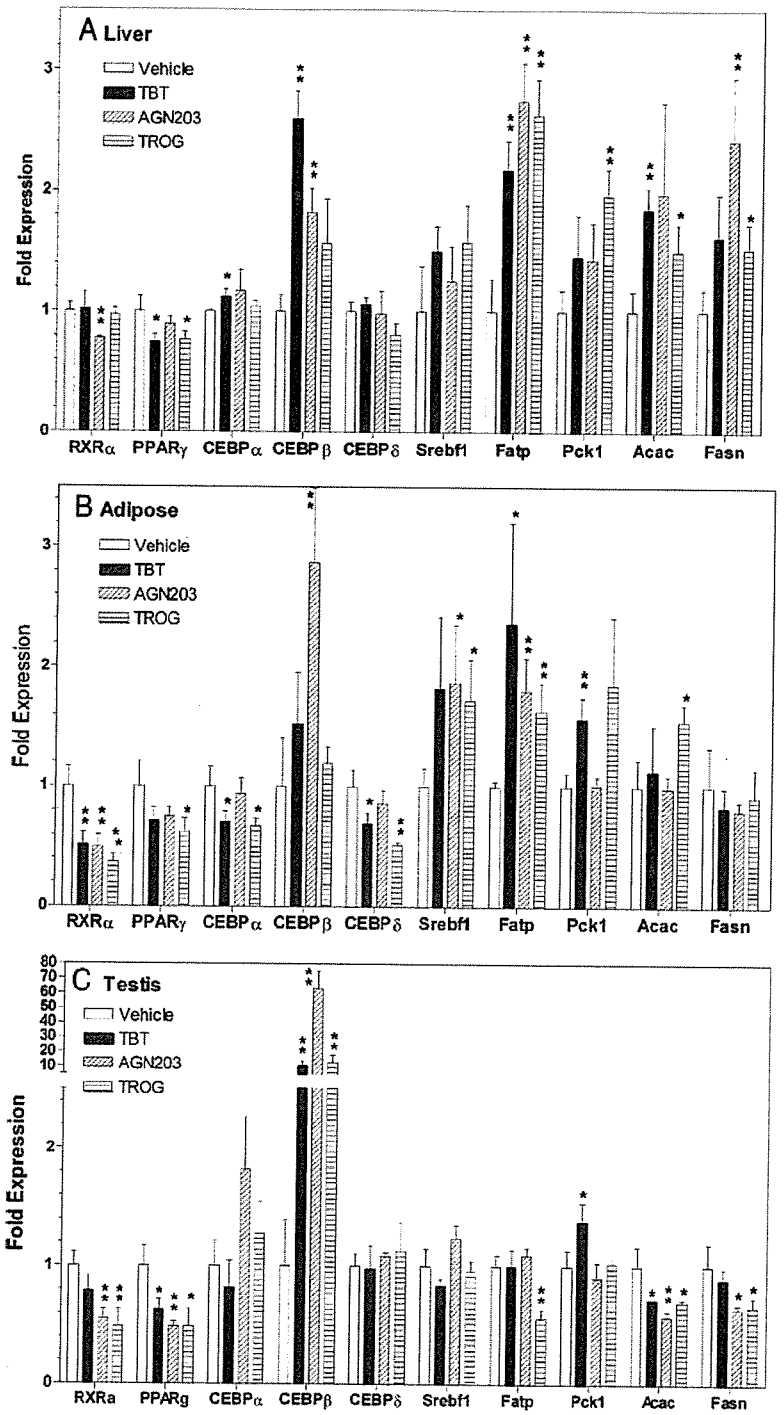

Fig. 3. *In Vivo* Induction of Adipogenic Modulators and RXR:PPARγ Target Genes

C57BL/6 male mice (three animals per treatment) were dosed with TBT (0.3 mg/kg b.w.), AGN195203 (0.3 mg/kg), troglitazone (3 mg/kg b.w.), or vehicle (corn oil) only by ip injection. Animals were killed after 24 h and dissected and cDNA was prepared from liver, epididymal fat pad, or testis for quantitative real-time PCR analysis. Expression levels were normalized to histone Hist2h4 and shown as the average fold change ± SEM (n = 3) compared with vehicle (corn oil) controls. Control *vs.* ligand treatments were analyzed by the unpaired Student's *t* test: *, $P < 0.1$; **, $P < 0.05$. TROG, Troglitazone.

with Oil Red O to assess changes in total tissue lipid accumulation. TBT exposure caused a disorganization of hepatic (Fig. 4, A and B) and gonadal (Fig. 4, C and D) architecture and significantly increased Oil Red O staining in treated animals *vs.* controls. Liver sections exhibited signs of steatosis consistent with the mis-

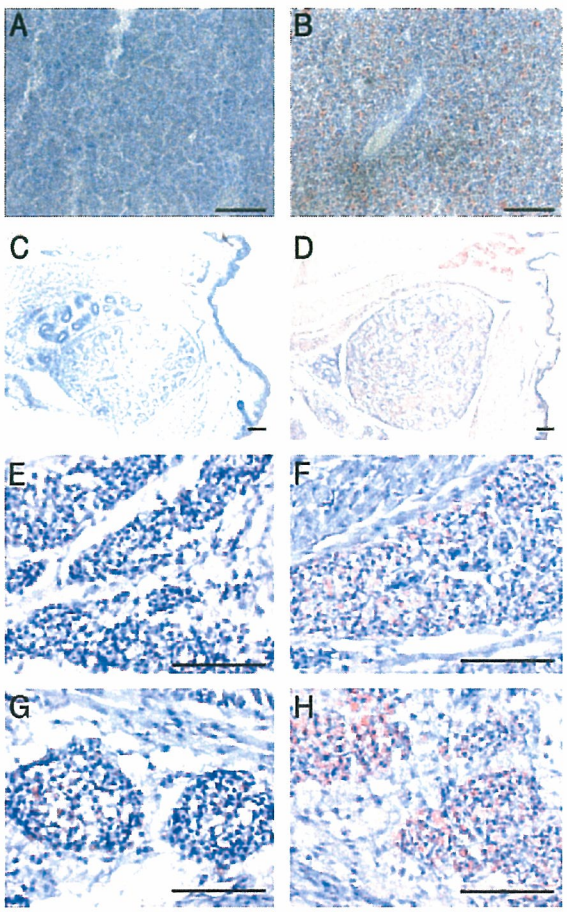

Fig. 4. *In Utero* Exposure to TBT Increases Adiposity in Mouse Liver, Testis, and Adipose Depots

Histological sections (12 μm) of newborn mouse liver (A and B), testis (C and D), inguinal adipose (E and F) and mammary adipose (G and H) stained with Oil Red O and counterstained with hematoxylin following *in utero* exposure to vehicle only (sesame oil) (A, C, E, and G) or 0.5 mg/kg b.w. TBT (B, D, F, and H) given s.c. daily from E12–18. *Scale bar*, 100 μm.

regulation of fatty acid uptake and synthesis observed using molecular markers. In addition, Oil Red O positive staining in mammary and inguinal adipose (Fig. 4, E–H) tissues was dramatically elevated, reflecting either an increase in lipid accumulation or an increase in mature adipocytes.

To determine whether exposure induced long-term changes in growth or adipose tissue, we followed mice from birth to adulthood after *in utero* exposure to TBT as indicated above. At birth, mice were cross-fostered to unexposed dams, and total body weight was recorded until 10 wk of age (Fig. 5A). Growth curves for male and female pups showed a slight trend for lower total body weight consistent with published observations (9) but were not statistically significant at 10 wk [control *vs.* TBT: male, 26.00 g ± 0.70 (n = 9) *vs.* 25.53 g ± 0.39 (n = 10), $P = 0.583$; female, 21.22 g ± 0.41 (n = 10), *vs.* 20.24 g ± 0.24 (n = 10), $P = 0.0529$]. Males were killed at 10 wk and epididymal fat pads were weighed (Fig. 5B). Adipose mass in TBT-treated males was increased significantly by 20% over controls [control *vs.* TBT: 0.30 g ± 0.020 (n = 9) *vs.* 0.36 g ± 0.018 (n = 10), $P = 0.0374$]. These data support the conclusion that TBT can increase body adiposity without overtly increasing total body weight. Similar lipid accumulation and changes in adipose tissue mass have also been observed after TZD or rexinoid treatment (55–57).

We had previously observed that TBT activated *Xenopus* RXRs (Table 1) and reasoned that the strong conservation in vertebrate nuclear receptor signaling pathways should result in consistent responses to organotin and RXR/PPARγ ligands across diverse vertebrate species. We therefore tested chronic exposure to environmentally relevant low doses of TBT (1–10 nM), the RXR-specific ligands LG100268 and AGN195203 (10–100 nM), troglitazone (0.1–1 μM), and estradiol (1–10 nM) on developing *X. laevis* tadpoles from stage 48 to metamorphs. To determine the effectiveness of these doses in *X. laevis* tadpoles, we used aromatase expression as a molecular marker because activity and expression are sensitive to endocrine disruption by organotins and RXR/PPARγ ligands in mammals (17, 18). *Xenopus* aromatase expression was similarly repressed 2- to 3-fold by 10 nM TBT, AGN195203, LG100268, or 1 μM troglitazone at stage 56 tadpoles (Fig. 6A) and at all subsequent stages. Despite significant ligand-induced aromatase down-regulation, neither sex ratios nor the time required to reach metamorphosis was altered (data not shown). *Xenopus* liver and kidney also exhibited no gross structural abnormalities at the doses given.

However, consistent with the testis and adipose results from mice presented above, we observed a dose-dependent increase in ectopic adipocyte formation posterior to the fat bodies in and around the gonads of both sexes after TBT or RXR/PPARγ ligand exposure (Fig. 6B). In contrast, estradiol-treated animals did not show increased adipocyte formation compared with controls. At 10 nM TBT, 10 nM AGN195203, or 1 μM troglitazone, ectopic adipocytes were observed in approximately 45–60% of animals. At the highest dose of TBT in males, testicular tissue was interspersed with, or replaced by, adipocytes along the anterior-posterior axis (Fig. 6, D, E, and G).

The concordant changes observed in *Xenopus* aromatase expression, gonadal adipocyte formation, and increased murine adiposity after exposure to TBT, RXR and PPARγ ligands are therefore consistent with a common mechanism of action through RXR:PPARγ activation, supporting the conclusion that endocrine disruption via nuclear receptor transcriptional regulation is a novel and key feature of organotin toxicity.

DISCUSSION

We have shown above that TBT is a potent inducer of adipogenesis, *in vitro* and *in vivo*, by acting as a novel,

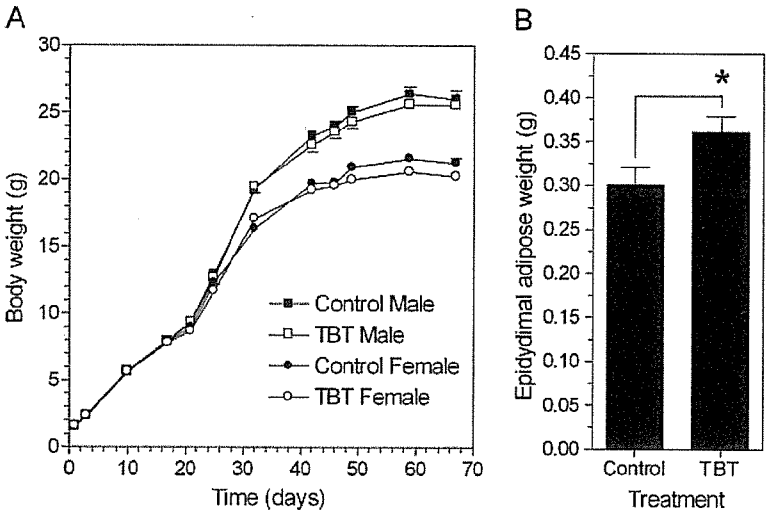

Fig. 5. *In Utero* Exposure to TBT Increases Adipose Mass But Not Body Weight in Adult Mice

A, Growth curves of C57BL/6 male and female pups exposed to control (sesame oil) or TBT *in utero* (E12–18). Data are mean ± SEM (n = 10). B, Epididymal fat pad weights from control or TBT-treated males at 10 wk. *, Epididymal adipose mass from exposed males was approximately 20% greater [control *vs.* TBT: 0.30 g ± 0.020 (n = 9) *vs.* 0.36 g ± 0.018 (n = 10); *, $P = 0.0374$). Data represent mean ± SEM (n = 9–10).

high-affinity xenobiotic ligand for RXRα and PPARγ. The ability of organotins to bind and activate these receptors, in particular the RXRs, which exhibit very restricted ligand specificity, is unexpected given the radically different chemical composition and three-dimensional molecular structure of organotins when compared with known natural and synthetic nuclear receptor ligands. Typically, RXR ligands comprise a carboxylic acid functional group and a three-dimensional molecular shape that mimics 9-*cis* RA. Structure-activity profiles indicate distinct structural preferences for organotins but also a relatively broad accommodation for agonist activity that is not easily reconciled with the classical ligand-binding model. Organotins may therefore interact somewhat differently than previously described RXR/PPARγ ligands with receptor LBDs to induce productive conformational changes required for coactivator recruitment. However, the binding data indicate that TBT is a potent and efficacious ligand for both RXRs and PPARγ that interacts, at least partially, with the same receptor-binding sites of other high-affinity ligands and promotes the necessary cofactor interactions required for agonist activation. In the study of Kanayama *et al.* (24), TBT was only effective in coactivator recruitment assays with PPARγ above 10 μM *in vitro*. However, in accord with our findings, they show that TBT activated PPARγ significantly at nanomolar concentrations in transfection assays. This may reflect a limitation of preference in the cofactor used *in vitro*. Alternatively, the lower maximal activation observed with TBT on PPARγ in cells (~30% at 100 nM TBT cf troglitazone) is consistent with one of two possibilities: either nonspecific cellular toxicity at high levels or activation as a partial agonist.

The ability of TBT to act as a dual ligand for permissive heterodimers such as RXRα:PPARγ, which can be activated by specific ligands for either receptor, also raises the possibility for additive or synergistic effects that might increase the potency of these compounds *in vivo* at low doses for this specific signaling pathway. Of note is that receptor activation is observed at nanomolar concentrations, whereas other mechanisms of toxicity and endocrine disruption, *e.g.* direct inhibition of aromatase activity, typically occur in the micromolar range. Furthermore, the activation of other permissive RXR heterodimeric partners, *e.g.* LXR and NURR1, suggests that organotins may act more widely to disrupt multiple nuclear receptor-mediated hormonal signaling pathways.

The biological consequences of organotin activation of the RXR:PPARγ signaling pathway are predictable and should follow known aspects of RXR/PPARγ biology. The RXR:PPARγ pathway plays a key role in adipocyte differentiation and energy storage, and is central to the control of whole-body metabolism (58). PPARγ activation increases the expression of genes that promote fatty acid storage and represses genes that induce lipolysis in adipocytes in white adipose tissue (59). PPARγ such as the thiazolidinediones can modulate insulin sensitivity due to these effects on the adipocyte, reversing insulin resistance in the whole body by sensitizing the muscle and liver tissue to insulin (60). However, a consequence of this increase in whole-body insulin sensitivity is that fat mass is increased through the promotion of triglyceride storage in adipocytes. Evidence is also mounting that depot-specific remodeling and adipocyte numbers increase after thiazolidinedione treatment (55–57). Therefore, PPARγ agonists comprise a class of phar-

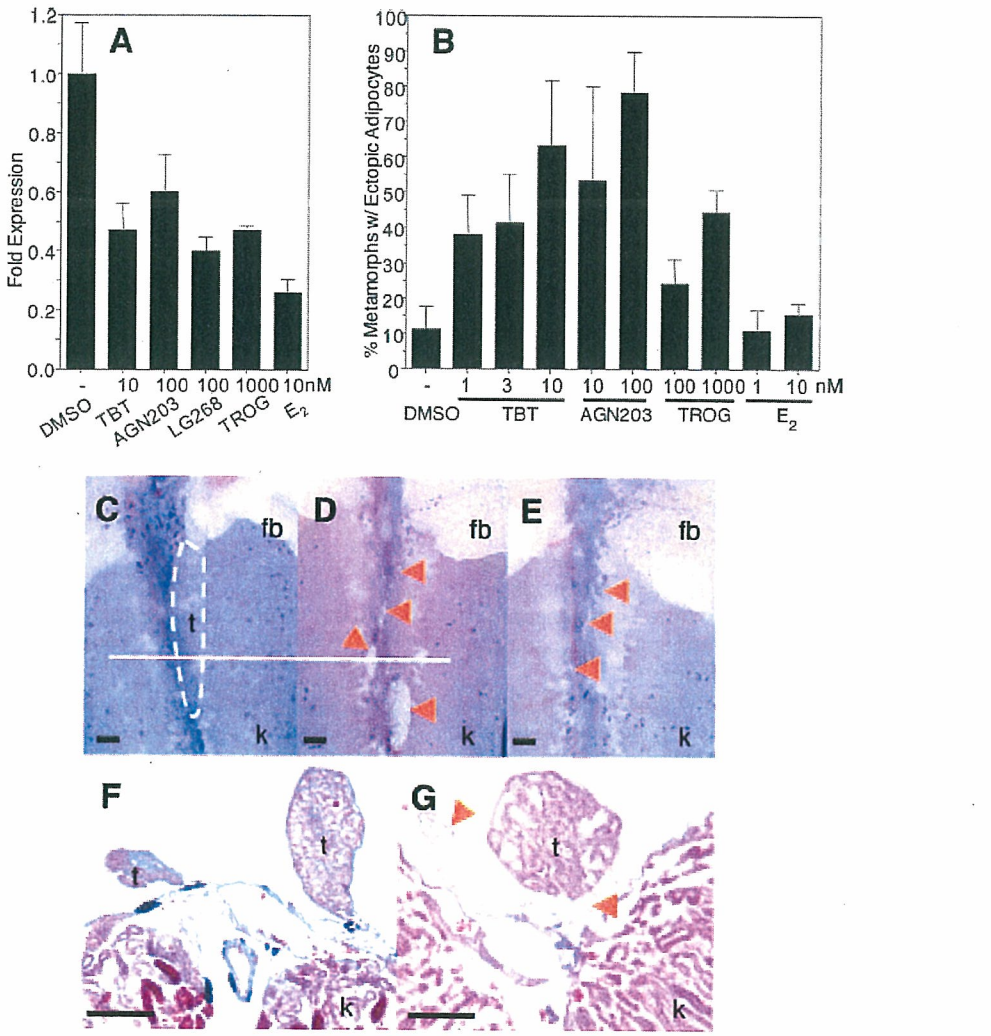

Fig. 6. Endocrine Disruption of RXR:PPARγ Signaling and Ectopic Induction of Adipocytes in *X. laevis* by TBT

A, Expression levels of *Xenopus* aromatase (XCYP19) were determined in tadpoles (stage 56) by quantitative real-time PCR after 24-h exposure to vehicle only (DMSO) or the indicated ligands. Expression was normalized to *Xenopus* EF1α and expressed as average fold change in expression ± SEM (n = 9) relative to vehicle controls. B, *X. laevis* tadpoles were dosed weekly under static renewal conditions with indicated ligands from stage 48 (before gonadogenesis) until stage 64 (metamorphic climax). Metamorphs (stage 66) were scored for ectopic adipocyte patches on gonads and urogenital ducts. Data are shown as the percentage of metamorphs exhibiting ectopic adipocyte patches posterior to the fat bodies; mean ± SD from triplicate tanks. C–E, Dissecting microscope photographs of kidneys (k), testis (t), and fat bodies (fb) from DMSO control, 10 nM TBT, and 1 μM troglitazone-treated male metamorphs. Multiple ectopic adipocyte patches (*red arrows*) are present posterior to the fat bodies along the anterior-posterior axis of gonads in TBT (D)- and troglitazone (E)-treated animals but not controls (C). Histological sections of kidneys and gonads from the same control (F) and 10 nM TBT (G)-treated males at the level indicated by the *white line* in C and D. Gonadal and connective tissue was either completely replaced by, or interspersed with, adipocytes (*red arrows*) in TBT-treated animals. Sections were developed with Mallory's trichrome stain. *Scale bars*, 100 μm.

maceutical therapies for type 2 diabetes that can also promote obesity by increasing fat storage. Likewise, RXR ligands also act as insulin-sensitizing agonists in rodents (61), underscoring the permissive nature of the PPARγ:RXR heterodimer and the potential effects on diabetes and obesity of both PPARγ and RXR agonists.

Our data are consistent with recent studies that organotins can mediate some of their endocrine disruption effects by transcriptional regulation through nuclear receptors, in particular RXR:PPARγ signaling (17–19, 24). Consequently, TBT exposure can promote adipocyte differentiation in the same manner as other RXR or PPARγ ligands *in vitro* using the standard murine 3T3-L1 cell model and *in vivo* through increased adiposity after intrauterine organotin exposure in newborn mice. It is currently unknown whether the increased adiposity *in vivo* results from an increase

in adipocyte precursor cell number, enhanced adipocyte differentiation from the same number of precursors, an increase in adipocyte size without an increase in number, or some combination of these.

The prevailing epidemiological data ascribe high-density caloric and/or fatty diets coupled with decreased physical activity as the root causes for the rise in obesity rates in the general population (62). The contribution of genetic components is less clear. Although genetic variation contributes to an individual's propensity to develop obesity, the rapid worldwide increase in obesity suggests that interaction with the modern environment exposes inherent genetic differences. The Barker hypothesis postulates that *in utero* fetal nutritional status is a potential risk factor for metabolic syndrome diseases (63–67). In this view, developmental metabolic programming of a thrifty phenotype limits the range in adaptive responses to the environment, *e.g.* diet and exercise, in later life (68). Experimental evidence from animal models lends support to this hypothesis (69). Plausible mechanisms include imprinting of obesity-sensitive hormonal pathways or changes in cell type and number, *e.g.* adipocytes, established during development.

Others, however, argue that the environment plays another role in obesity. Because the increase in obesity rates parallels the rapid growth in the use of industrial chemicals over the past 40 yr, it is plausible and provocative to associate *in utero* or chronic lifetime exposure to chemical triggers present in the modern environment with this epidemic. Hence, an "obesogen" model predicts the existence of xenobiotic chemicals that inappropriately regulate lipid metabolism and adipogenesis to promote obesity. Several recent studies serve as proof-of-principle for such a hypothesis. Environmental estrogens such as bisphenol A and nonylphenol, for instance, can promote adipocyte differentiation or proliferation in murine cell lines (70, 71). Furthermore, epidemiological studies link maternal smoking during pregnancy to an elevated risk of childhood obesity (72–76).

Seen in this context, we propose that organotins such as TBT and its congeners are chemical stressors or obesogens that activate RXR:PPARγ signaling to promote long-term changes in adipocyte number and/or lipid homeostasis after developmental or chronic lifetime exposure.

MATERIALS AND METHODS

Plasmids and Transfections

pCMX-GAL4 and pCMX-VP16 plasmid fusion constructs to nuclear receptor LBDs and coactivators [GAL4-hRARα, hRXRα, -xRXRα/γ, -hPPARγ, -mPPARα, -human steroid and xenobiotic receptor (SXR), -NURR1, -VDR, -LXR, -hACTR, -hPPAR-binding protein (PBP), -human steroid receptor coactivator-1 (SRC-1), human transcriptional intermediary factor 2 (TIF2)] have been previously described (77–82). Transfections were performed in Cos7 cells (transformed green monkey kidney fibroblast cell line) essentially as described elsewhere (83) using MH200-x4-TK-Luc as reporter and normalized to pCMX-β-galactosidase controls. Briefly, Cos7 cells were seeded at 5000 cells per well in 96-well tissue culture plates in 10% fetal bovine serum/DMEM and transfected for 8 h with 11 μg/plate of DNA/calcium phosphate precipitate mix (MH200x4-TK-Luc-CMX-β-galactosidase-nuclear receptor/coactivator effector(s) at a ratio of 5:5:1). Cells were washed free of precipitate with PBS and media were replaced with serum-free insulin, transferrin, lipid, bovine serum albumin supplemented (ITLB)/DMEM (84) plus ligands for an additional 24 h before assays for luciferase and β-galactosidase activity. All transfection data points were performed in triplicate, and all experiments were repeated at least three times.

Quantitative Real-Time PCR Analyses

Total cellular RNA from C57BL/6 mouse and *X. laevis* tissues was isolated with Trizol reagent and reversed transcribed with oligo dT and Superscript II (Invitrogen, San Diego, CA) according to the manufacturer's instructions. Triplicate cDNA samples (50 ng/reaction) were analyzed by quantitative real-time PCR on a DNA Engine Opticon thermal cycler [MJ Research (Watertown, MA)/Bio-Rad Laboratories (Hercules, CA)] using SYBR Green chemistry (PerkinElmer Life Sciences, Wellesley, MA). Fold changes in expression levels were calculated after normalization to histone Hist2h4 using the Δ-Δ cycle threshold method (85). Gene-specific primers were as follows. Hist2h4 forward (F): 5′-CCCGTGGTGTGCTGAAGGTGTT-3′; reverse (R), 5′-GAATTGAAGCGGCGGCGTCTA-3′; RXRα F: 5′-CGGCTGCTCAGGGTACTTGTGTTT-3′; R, 5′-CGGCTGCTCAGGGTACTTGTGTTT-3′; PPARγ F: 5′-TGGGTGAAACTCTGGGAGATTC-3′; R, 5′-AATTTCTTGTGAAGTGCTCATAGGC-3′; C/EBPα F: 5′-CCAAGAAGTCGGTGGACAAGA-3′; R, 5′-CGGTCATTGTCACTGGTCAACT-3′; C/EBPβ F: 5′-GCCCGCCGCCTTTAGACC-3′; R, 5′-CGCTCGTGCTCGCCAATG-3′; C/EBPδ F: 5′-AACCCGCGGCCTTCTACGAG-3′; R, 5′-ACGGCGGCCATGGAGTCAAT-3′; aP2 F: 5′-GAATTCGATGAAATCACCGCA-3′; R, 5′-CTCTTTATTGTGGTCGACTTTCCA-3′; FATP F: 5′-AGCCGCTTCTGGGATGACTGTGT-3′; R, 5′-ACCGAAGCGCTGCGTGAACTC-3′; ACS F: 5′-CCCAGCCAGTCCCCACCAG-3′; R, 5′-CACACCACTCAGGCTCACACTCGT-3′; FASN F: 5′-TCGGGTGTGGTGGGTTTGGTGAAT-3′; R, 5′-ACTTGGGGGCGTGAGATGTGTTGC-3′;ACAC F: 5′-G GATGGCAGCTCTGGAGGTGTATG-3′; R, 5′-TGTCCTTAAGCTGGCGGTGTTGTA; Pck1 F: 5′-CTGGCAGCATGGGGTGTTTGTAGG-3′; R, 5′-TGCCGAAGTTGTAGCCGAAGAAGG-3′; Srebf1 F: 5′-GCCCCTGCCCACCTCAAACCT-3′; R, 5′-ACTGGCACGGGCATCCTTCCTC-3′; *Xenopus* EF1α F: 5′-GATCCCAGGAAAGCCAATGTGC 3′; R, 5′-CCGGATCCTGCTGCCTTCTTCT-3′; *Xenopus* CYP19 (aromatase) F: 5′-GTCTGGATTAATGGCGAGGAAACA-3′; R, 5′-CTGATGAAGTATGGCCGAATGACC-3′.

Ligand Binding

Histidine-tagged RXRα LBD (H_6-RXRα LBDs) was expressed and purified from pET15b(+) vector in BL21(DE3) pLysS bacteria cultures after induction with 1 mM isopropyl-β-D-thiogalactopyranoside for 3 h at 37 C (86). Purified H_6-PPARγ was purchased from Invitrogen. Proteins were bound to 96-well Nickel Chelate Flashplates (PerkinElmer Life Sciences) at 100 μg/ml overnight at 4 C and washed five times with 200 μl/well Flashplate Assay Buffer (20 mM HEPES, pH 7.9; 100 mM KCl, 0.1% cholamidopropyldimethylammonio-2-hydroxy-1-propanesulfonate, 0.1 mM dithiothreitol). Competition assays typically used 1–5 nM [^{3}H]-9-*cis*-RA (PerkinElmer Life Sciences) or 10–50 nM [^{3}H]rosiglitazone (American Radiochemicals, Inc., St. Louis, MO) plus cold competitor ligands in Flashplate Assay Buffer at concentrations indicated in the figures. Plates were incubated at room temperature, pro-

tected from light, and read after 4 h on a Packard Topcount scintillation counter (Packard Instruments, Meriden, CT). Specific bound counts/min were determined by subtraction of counts/min from uncoated wells at each ligand concentration. Data were analyzed with GraphPad Prism 4.0 (GraphPad Software, Inc., San Diego, CA) using a one-site competition binding equation to determine K_i values for competitor ligands; K_d values of 1.4 and 41 nM for 9-*cis*-RA and rosiglitazone for their respective receptors were used in the calculations (87, 88).

3T3-L1 Cell Assays

3T3-L1 (American Type Culture Collection, Manassas, VA) cells were maintained as subconfluent cultures by passage every 3 d from cultures seeded at 5000 cells/cm^2 in 8% calf serum/DMEM. For differentiation assays, cells were seeded at 15×10^3 cells per well into 24-well tissue culture plates in 8% fetal bovine serum/DMEM, after which cultures were grown for 2 d and then treated with the indicated RXR, RAR, and PPAR ligands either with or without MDIT (100 μM 3-isobutyl-1-methylxanthine, 100 nM dexamethasone, 0.1 ng/ml insulin, and 2 nM T_3 thyroid hormone) induction cocktail. Media and ligand treatments were renewed every 2 d. After 1 wk, cells were scored for adipocyte differentiation by Oil Red O staining for lipid droplet accumulation. Cultures were washed with PBS, fixed with 10% formaldehyde for 15 min, washed with distilled water, and stained with filtered Oil Red O solution (4 g/liter, 60% isopropanol) for 15 min. Excess stain was removed by washing three times with distilled water. Three random fields from each well were photographed under phase contrast and analyzed in ImageJ. Images were converted into high-contrast black and white images to visualize lipid droplets and scored as the percentage area per field. Data are shown as the mean ± SEM from three wells per treatment. The method was validated by extraction of Oil Red O from stained cells into 100% isopropanol and quantitated by absorbance at 540 nm on a spectrophotometer.

In Vivo Animal Exposure Experiments

C57BL/6J mice were housed under a 12-h light, 12-h dark cycle. Pregnant mice were dosed by ip injection with TBT [0.05 or 0.5 mg/kg body weight (b.w.)] or vehicle (sesame oil) from embryonic d 12 (E12) every 24 h until the day before delivery. Neonates were killed at the day of delivery and analyzed. The samples were embedded in optimal cutting temperature embedding compound and sectioned (12 mm) using a cryostat. Sections were fixed on slides with 4% paraformaldehyde for 10 min and rinsed in PBS. The slides were then sequentially washed with distilled water and 60% of isopropanol and stained with Oil Red O (4 g/liter, 60% isopropanol). After washing with 60% isopropanol and distilled water, the slides were counterstained with hematoxylin. Sections were evaluated and photographed using a Zeiss microscope (Carl Zeiss, Thornwood, NY).

For long-term growth studies, pups were cross-fostered to unexposed C57BL/6 dams after birth, and litter sizes were kept constant at eight pups per dam (control, two male + two female; TBT treated, two male + two female). Animals were weaned at 3 wk of age and maintained on standard rodent chow. Total body weight was followed until 10 wk of age. Males were then killed, and epididymal fat pads were dissected and weighed.

X. laevis tadpoles were sorted at stage 48 (89) and maintained in 1-liter glass tanks in 20% Holtfreter's buffered salt solution (90) at a density of 10 tadpoles per tank on a diet of ground Tetramin Fish Flakes and spirulina. Compounds prepared in dimethylsulfoxide (DMSO) as 10^5-fold stock solutions were tested on triplicate tanks and dosed by static renewal after weekly water changes. Metamorphs at stage 64 were transferred to individual containers and fed frozen brine shrimp for 2 wk until stage 66. Froglets were euthanized with 250 mg/liter MS222 in 20% Holtfreter's solution and then scored for gonadal abnormalities and interrenal/gonadal adipocyte formation under a dissecting microscope. Kidneys with attached gonads and livers were fixed in 10% formalin-PBS, embedded in paraffin, and sectioned at 15 μm thickness. Sections were developed with Mallory's trichrome stain.

All animal experiments were approved and performed in accordance with Institutional Animal Care and Use Committee protocols.

Acknowledgments

We thank Drs. I. Blitz, K. Cho, C. Zhou, and T. Osborne for critical reading and comments on the manuscript, Dr. C. Li (Expression Technologies) for the H_6-RXRα LBD construct, and Dr. R. Chandraratna (Allergan Pharmaceuticals, Irvine, CA) for AGN203 and LG268).

Received September 8, 2005. Accepted March 30, 2006.

Address all correspondence and requests for reprints to: Bruce Blumberg, Department of Developmental and Cell Biology, University of California Irvine, 2113 McGaugh Hall, Irvine, California 92697-2300. E-mail: blumberg@uci.edu.

This work was supported by grants from the U.S. Environmental Protection Agency (STAR R830686) and National Institutes of Health (GM-60572) (to B.B.); from the Ministries of Education, Culture, Sports, Science and Technology, Environment and Health Labor and Welfare, Japan (to T.I.); and from the University of California Toxic Substance Research and Training Program (UC-37579) (to F.G.).

F.G., H.W., Z.Z., L.M., K.A., R.C., D.M.G., J.K., T.I. have nothing to declare. B.B. is a named inventor on U.S. patents US 5,861,274, US 6,200,802, and US 6,815,168.

REFERENCES

1. Appel KE 2004 Organotin compounds: toxicokinetic aspects. Drug Metab Rev 36:763–786
2. Golub M, Doherty J 2004 Triphenyltin as a potential human endocrine disruptor. J Toxicol Environ Health B Crit Rev 7:281–295
3. Blaber SJM 1970 The occurrence of a penis-like outgrowth behind the right tentacle in spent females of *Nucella lapillus*. Proc Malacolog Soc London 39:231–233
4. Gibbs P, Bryan G 1986 Reproductive failure in populations of the dog-whelk, *Nucella lapillus*, caused by imposex induced by tributyltin from antifouling paints. J Mar Biol Assoc UK 66:767–777
5. Matthiessen P, Gibbs P 1998 Critical appraisal of the evidence for tributyltin-mediated endocrine disruption in mollusks. Environ Toxicol Chem 17:37–43
6. Shimasaki Y, Kitano T, Oshima Y, Inoue S, Imada N, Honjo T 2003 Tributyltin causes masculinization in fish. Environ Toxicol Chem 22:141–144
7. McAllister BG, Kime DE 2003 Early life exposure to environmental levels of the aromatase inhibitor tributyltin causes masculinisation and irreversible sperm damage in zebrafish (*Danio rerio*). Aquat Toxicol 65:309–316
8. Omura M, Ogata R, Kubo K, Shimasaki Y, Aou S, Oshima Y, Tanaka A, Hirata M, Makita Y, Inoue N 2001 Two-generation reproductive toxicity study of tributyltin chloride in male rats. Toxicol Sci 64:224–232
9. Ogata R, Omura M, Shimasaki Y, Kubo K, Oshima Y, Aou S, Inoue N 2001 Two-generation reproductive toxicity

study of tributyltin chloride in female rats. J Toxicol Environ Health A 63:127–144
10. Boyer IJ 1989 Toxicity of dibutyltin, tributyltin and other organotin compounds to humans and to experimental animals. Toxicology 55:253–298
11. Heidrich DD, Steckelbroeck S, Klingmuller D 2001 Inhibition of human cytochrome P450 aromatase activity by butyltins. Steroids 66:763–769
12. Cooke GM 2002 Effect of organotins on human aromatase activity in vitro. Toxicol Lett 126:121–130
13. Powers MF, Beavis AD 1991 Triorganotins inhibit the mitochondrial inner membrane anion channel. J Biol Chem 266:17250–17256
14. Gennari A, Viviani B, Galli CL, Marinovich M, Pieters R, Corsini E 2000 Organotins induce apoptosis by disturbance of [Ca(2+)](i) and mitochondrial activity, causing oxidative stress and activation of caspases in rat thymocytes. Toxicol Appl Pharmacol 169:185–190
15. Philbert MA, Billingsley ML, Reuhl KR 2000 Mechanisms of injury in the central nervous system. Toxicol Pathol 28:43–53
16. Mu YM, Yanase T, Nishi Y, Waseda N, Oda T, Tanaka A, Takayanagi R, Nawata H 2000 Insulin sensitizer, troglitazone, directly inhibits aromatase activity in human ovarian granulosa cells. Biochem Biophys Res Commun 271:710–713
17. Mu YM, Yanase T, Nishi Y, Takayanagi R, Goto K, Nawata H 2001 Combined treatment with specific ligands for PPARγ:RXR nuclear receptor system markedly inhibits the expression of cytochrome P450arom in human granulosa cancer cells. Mol Cell Endocrinol 181:239–248
18. Saitoh M, Yanase T, Morinaga H, Tanabe M, Mu YM, Nishi Y, Nomura M, Okabe T, Goto K, Takayanagi R, Nawata H 2001 Tributyltin or triphenyltin inhibits aromatase activity in the human granulosa-like tumor cell line KGN. Biochem Biophys Res Commun 289:198–204
19. Nishikawa J, Mamiya S, Kanayama T, Nishikawa T, Shiraishi F, Horiguchi T 2004 Involvement of the retinoid X receptor in the development of imposex caused by organotins in gastropods. Environ Sci Technol 38: 6271–6276
20. Baillie-Hamilton PF 2002 Chemical toxins: a hypothesis to explain the global obesity epidemic. J Altern Complement Med 8:185–192
21. Heindel JJ 2003 Endocrine disruptors and the obesity epidemic. Toxicol Sci 76:247–249
22. Jacobs MN, Lewis DF 2002 Steroid hormone receptors and dietary ligands: a selected review. Proc Nutr Soc 61:105–122
23. Watanabe H, Iguchi T, Morohashi K 2002 [Endocrine disruptors and nuclear receptors]. Nippon Rinsho 60: 397–403
24. Kanayama T, Kobayashi N, Mamiya S, Nakanishi T, Nishikawa J 2005 Organotin compounds promote adipocyte differentiation as agonists of the peroxisome proliferator-activated receptor γ/retinoid X receptor pathway. Mol Pharmacol 67:766–774
25. Wang Z, Benoit G, Liu J, Prasad S, Aarnisalo P, Liu X, Xu H, Walker NP, Perlmann T 2003 Structure and function of Nurr1 identifies a class of ligand-independent nuclear receptors. Nature 423:555–560
26. Aarnisalo P, Kim CH, Lee JW, Perlmann T 2002 Defining requirements for heterodimerization between the retinoid X receptor and the orphan nuclear receptor Nurr1. J Biol Chem 277:35118–35123
27. Boehm MF, Zhang L, Zhi L, McClurg MR, Berger E, Wagoner M, Mais DE, Suto CM, Davies JA, Heyman RA, Nadzant AM 1995 Design and synthesis of potent retinoid X receptor selective ligands that induce apoptosis in leukemia cells. J Med Chem 38:3146–3155
28. Yu C, Chen L, Luo H, Chen J, Cheng F, Gui C, Zhang R, Shen J, Chen K, Jiang H, Shen X 2004 Binding analyses between human PPARγ-LBD and ligands. Eur J Biochem 271:386–397
29. Forman BM, Tontonoz P, Chen J, Brun RP, Spiegelman BM, Evans RM 1995 15-Deoxy-δ 12, 14-prostaglandin J2 is a ligand for the adipocyte determination factor PPAR γ. Cell 83:803–812
30. Schoonjans K, Staels B, Auwerx J 1996 The peroxisome proliferator activated receptors (PPARs) and their effects on lipid metabolism and adipocyte differentiation. Biochim Biophys Acta 1302:93–109
31. Kersten S 2002 Peroxisome proliferator activated receptors and obesity. Eur J Pharmacol 440:223–234
32. Lane MD, Tang QQ, Jiang MS 1999 Role of the CCAAT enhancer binding proteins (C/EBPs) in adipocyte differentiation. Biochem Biophys Res Commun 266:677–683
33. Tang QQ, Otto TC, Lane MD 2003 CCAAT/enhancer-binding protein β is required for mitotic clonal expansion during adipogenesis. Proc Natl Acad Sci USA 100: 850–855
34. Tang QQ, Lane MD 1999 Activation and centromeric localization of CCAAT/enhancer-binding proteins during the mitotic clonal expansion of adipocyte differentiation. Genes Dev 13:2231–2241
35. Rubin CS, Hirsch A, Fung C, Rosen OM 1978 Development of hormone receptors and hormonal responsiveness in vitro. Insulin receptors and insulin sensitivity in the preadipocyte and adipocyte forms of 3T3–L1 cells. J Biol Chem 253:7570–7578
36. Kletzien RF, Clarke SD, Ulrich RG 1992 Enhancement of adipocyte differentiation by an insulin-sensitizing agent. Mol Pharmacol 41:393–398
37. Kletzien RF, Foellmi LA, Harris PK, Wyse BM, Clarke SD 1992 Adipocyte fatty acid-binding protein: regulation of gene expression in vivo and in vitro by an insulin-sensitizing agent. Mol Pharmacol 42:558–562
38. Tafuri SR 1996 Troglitazone enhances differentiation, basal glucose uptake, and Glut1 protein levels in 3T3–L1 adipocytes. Endocrinology 137:4706–4712
39. Xue JC, Schwarz EJ, Chawla A, Lazar MA 1996 Distinct stages in adipogenesis revealed by retinoid inhibition of differentiation after induction of PPARγ. Mol Cell Biol 16:1567–1575
40. Kawada T, Kamei Y, Sugimoto E 1996 The possibility of active form of vitamins A and D as suppressors on adipocyte development via ligand-dependent transcriptional regulators. Int J Obes Relat Metab Disord 20(Suppl 3):S52–S57
41. Kawada T, Kamei Y, Fujita A, Hida Y, Takahashi N, Sugimoto E, Fushiki T 2000 Carotenoids and retinoids as suppressors on adipocyte differentiation via nuclear receptors. Biofactors 13:103–109
42. Tontonoz P, Graves RA, Budavari AI, Erdjument-Bromage H, Lui M, Hu E, Tempst P, Spiegelman BM 1994 Adipocyte-specific transcription factor ARF6 is a heterodimeric complex of two nuclear hormone receptors, PPAR γ and RXR α. Nucleic Acids Res 22:5628–5634
43. Martin G, Schoonjans K, Lefebvre AM, Staels B, Auwerx J 1997 Coordinate regulation of the expression of the fatty acid transport protein and acyl-CoA synthetase genes by PPARα and PPARγ activators. J Biol Chem 272:28210–28217
44. Motojima K, Passilly P, Peters JM, Gonzalez FJ, Latruffe N 1998 Expression of putative fatty acid transporter genes are regulated by peroxisome proliferator-activated receptor α and γ activators in a tissue- and inducer-specific manner. J Biol Chem 273:16710–16714
45. Frohnert BI, Hui TY, Bernlohr DA 1999 Identification of a functional peroxisome proliferator-responsive element in the murine fatty acid transport protein gene. J Biol Chem 274:3970–3977
46. Martin G, Poirier H, Hennuyer N, Crombie D, Fruchart JC, Heyman RA, Besnard P, Auwerx J 2000 Induction of the fatty acid transport protein 1 and acyl-CoA synthase

genes by dimer-selective rexinoids suggests that the peroxisome proliferator-activated receptor-retinoid X receptor heterodimer is their molecular target. J Biol Chem 275:12612–12618
47. Tontonoz P, Hu E, Devine J, Beale EG, Spiegelman BM 1995 PPAR γ 2 regulates adipose expression of the phosphoenolpyruvate carboxykinase gene. Mol Cell Biol 15:351–357
48. Magana MM, Lin SS, Dooley KA, Osborne TF 1997 Sterol regulation of acetyl coenzyme A carboxylase promoter requires two interdependent binding sites for sterol regulatory element binding proteins. J Lipid Res 38: 1630–1638
49. Schadinger SE, Bucher NL, Schreiber BM, Farmer SR 2005 PPARγ2 regulates lipogenesis and lipid accumulation in steatotic hepatocytes. Am J Physiol Endocrinol Metab 288:E1195–E1205
50. Tontonoz P, Kim JB, Graves RA, Spiegelman BM 1993 ADD1: a novel helix-loop-helix transcription factor associated with adipocyte determination and differentiation. Mol Cell Biol 13:4753–4759
51. Kim JB, Spiegelman BM 1996 ADD1/SREBP1 promotes adipocyte differentiation and gene expression linked to fatty acid metabolism. Genes Dev 10:1096–1107
52. Joseph SB, Laffitte BA, Patel PH, Watson MA, Matsukuma KE, Walczak R, Collins JL, Osborne TF, Tontonoz P 2002 Direct and indirect mechanisms for regulation of fatty acid synthase gene expression by liver X receptors. J Biol Chem 277:11019–11025
53. Seo JB, Moon HM, Kim WS, Lee YS, Jeong HW, Yoo EJ, Ham J, Kang H, Park MG, Steffensen KR, Stulnig TM, Gustafsson JA, Park SD, Kim JB 2004 Activated liver X receptors stimulate adipocyte differentiation through induction of peroxisome proliferator-activated receptor γ expression. Mol Cell Biol 24:3430–3444
54. Yu S, Matsusue K, Kashireddy P, Cao WQ, Yeldandi V, Yeldandi AV, Rao MS, Gonzalez FJ, Reddy JK 2003 Adipocyte-specific gene expression and adipogenic steatosis in the mouse liver due to peroxisome proliferator-activated receptor γ1 (PPARγ1) overexpression. J Biol Chem 278:498–505
55. Hallakou S, Doare L, Foufelle F, Kergoat M, Guerre-Millo M, Berthault MF, Dugail I, Morin J, Auwerx J, Ferre P 1997 Pioglitazone induces in vivo adipocyte differentiation in the obese Zucker fa/fa rat. Diabetes 46:1393–1399
56. de Souza CJ, Eckhardt M, Gagen K, Dong M, Chen W, Laurent D, Burkey BF 2001 Effects of pioglitazone on adipose tissue remodeling within the setting of obesity and insulin resistance. Diabetes 50:1863–1871
57. Smith SR, De Jonge L, Volaufova J, Li Y, Xie H, Bray GA 2005 Effect of pioglitazone on body composition and energy expenditure: a randomized controlled trial. Metabolism 54:24–32
58. Auwerx J 1999 PPARγ, the ultimate thrifty gene. Diabetologia 42:1033–1049
59. Ferre P 2004 The biology of peroxisome proliferator-activated receptors: relationship with lipid metabolism and insulin sensitivity. Diabetes 53(Suppl 1):S43–S50
60. Day C 1999 Thiazolidinediones: a new class of antidiabetic drugs. Diabet Med 16:179–192
61. Mukherjee R, Davies PJ, Crombie DL, Bischoff ED, Cesario RM, Jow L, Hamann LG, Boehm MF, Mondon CE, Nadzan AM, Paterniti Jr JR, Heyman RA 1997 Sensitization of diabetic and obese mice to insulin by retinoid X receptor agonists. Nature 386:407–410
62. Hill JO, Peters JC 1998 Environmental contributions to the obesity epidemic. Science 280:1371–1374
63. Barker DJ, Bull AR, Osmond C, Simmonds SJ 1990 Fetal and placental size and risk of hypertension in adult life. Br Med J 301:259–262
64. Phillips DI, Hirst S, Clark PM, Hales CN, Osmond C 1994 Fetal growth and insulin secretion in adult life. Diabetologia 37:592–596
65. Martyn CN, Barker DJ, Jespersen S, Greenwald S, Osmond C, Berry C 1995 Growth in utero, adult blood pressure, and arterial compliance. Br Heart J 73:116–121
66. Yajnik C 2000 Interactions of perturbations in intrauterine growth and growth during childhood on the risk of adult-onset disease. Proc Nutr Soc 59:257–265
67. Barker DJ, Martyn CN, Osmond C, Hales CN, Fall CH 1993 Growth in utero and serum cholesterol concentrations in adult life. Br Med J 307:1524–1527
68. Lucas A 1998 Programming by early nutrition: an experimental approach. J Nutr 128:401S–406S
69. Armitage JA, Khan IY, Taylor PD, Nathanielsz PW, Poston L 2004 Developmental programming of metabolic syndrome by maternal nutritional imbalance; how strong is the evidence from experimental models in mammals? J Physiol 561:355–377
70. Masuno H, Kidani T, Sekiya K, Sakayama K, Shiosaka T, Yamamoto H, Honda K 2002 Bisphenol A in combination with insulin can accelerate the conversion of 3T3–L1 fibroblasts to adipocytes. J Lipid Res 43:676–684
71. Masuno H, Okamoto S, Iwanami J, Honda K, Shiosaka T, Kidani T, Sakayama K, Yamamoto H 2003 Effect of 4-nonylphenol on cell proliferation and adipocyte formation in cultures of fully differentiated 3T3–L1 cells. Toxicol Sci 75:314–320
72. Toschke AM, Koletzko B, Slikker Jr W, Hermann M, von Kries R 2002 Childhood obesity is associated with maternal smoking in pregnancy. Eur J Pediatr 161:445–448
73. von Kries R, Toschke AM, Koletzko B, Slikker Jr W 2002 Maternal smoking during pregnancy and childhood obesity. Am J Epidemiol 156:954–961
74. Oken E, Huh SY, Taveras EM, Rich-Edwards JW, Gillman MW 2005 Associations of maternal prenatal smoking with child adiposity and blood pressure. Obes Res 13: 2021–2028
75. Power C, Jefferis BJ 2002 Fetal environment and subsequent obesity: a study of maternal smoking. Int J Epidemiol 31:413–419
76. Hill SY, Shen S, Locke Wellman J, Rickin E, Lowers L 2005 Offspring from families at high risk for alcohol dependence: increased body mass index in association with prenatal exposure to cigarettes but not alcohol. Psychiatry Res 135:203–216
77. Umesono K, Murakami KK, Thompson CC, Evans RM 1991 Direct repeats as selective response elements for the thyroid hormone, retinoic acid, and vitamin D3 receptors. Cell 65:1255–1266
78. Perlmann T, Rangarajan PN, Umesono K, Evans RM 1993 Determinants for selective RAR and TR recognition of direct repeat HREs. Genes Dev 7:1411–1422
79. Blumberg B, Mangelsdorf DJ, Dyck JA, Bittner DA, Evans RM, De Robertis EM 1992 Multiple retinoid-responsive receptors in a single cell: families of retinoid "X" receptors and retinoic acid receptors in the *Xenopus* egg. Proc Natl Acad Sci USA 89:2321–2325
80. Blumberg B, Bolado J Jr., Derguini F, Craig AG, Moreno TA, Chakravarti D, Heyman RA, Buck J, Evans RM 1996 Novel retinoic acid receptor ligands in *Xenopus* embryos. Proc Natl Acad Sci USA 93:4873–4878
81. Blumberg B, Sabbagh Jr W, Juguilon H, Bolado Jr J, van Meter CM, Ong ES, Evans RM 1998 SXR, a novel steroid and xenobiotic-sensing nuclear receptor. Genes Dev 12: 3195–3205
82. Tabb MM, Sun A, Zhou C, Grun F, Errandi J, Romero K, Pham H, Inoue S, Mallick S, Lin M, Forman BM, Blumberg B 2003 Vitamin K2 regulation of bone homeostasis is mediated by the steroid and xenobiotic receptor SXR. J Biol Chem 278:43919–43927
83. Grun F, Blumberg B 2003 Identification of novel nuclear hormone receptor ligands by activity-guided purification. Methods Enzymol 364:3–24
84. Grun F, Venkatesan RN, Tabb MM, Zhou C, Cao J, Hemmati D, Blumberg B 2002 Benzoate X receptors α